12-18-2011

Testing the Limits of Hyperspectral Airborne Remote Sensing by Mapping Eelgrass in Elkhorn Slough

Kelley J. Bostrom
University of Connecticut - Avery Point, kelley.bostrom@uconn.edu

Testing the Limits of Hyperspectral Airborne Remote Sensing by Mapping Eelgrass in Elkhorn Slough

Kelley Jean Bostrom

B.A., Brandeis University, 2008

A Thesis
Submitted in Partial Fulfillment of the
Requirements for the Degree of
Master of Science
at the
University of Connecticut
2011

APPROVAL PAGE

Master of Science Thesis

Testing the Limits of Hyperspectral Airborne Remote Sensing by

Mapping Eelgrass in Elkhorn Slough

Presented by

Kelley Jean Bostrom, B.A.

Major Advisor _____

Heidi M. Dierssen

Associate Advisor _____

Robert B. Whitlatch

Associate Advisor _____

Michael M. Whitney

University of Connecticut

2011

ACKNOWLEDGEMENTS

There are many people without whom this project would not have been possible. First and foremost, I would like to thank my advisor, Dr. Heidi Dierssen. Heidi has provided support and guidance throughout my graduate career, and I have learned a great deal from her. In addition to my work on my thesis, she has given me the opportunity to travel, work, and learn beyond my research focus. I would also like to recognize my committee members, Dr. Robert Whitlatch and Dr. Michael Whitney, for offering their time and insight.

For their contributions to my research project, I would like to thank the Florida Environmental Research Institute, specifically Paul Bissett and the SAMSON imagery team. Additional data used in this study were acquired, processed, archived, and distributed by the Seafloor Mapping Lab of California State University Monterey Bay. Thanks also to Chris Buonassissi and Jeff Godfrey for their work in data collection and their help in answering my questions as I began my work on the project. To the ITT Visual Information Solutions Technical Support team, for further assistance with writing data processing code. To the COLORS Lab, Dirk Aurin, Kate Randolph, and Brandon Russell, for help and advice with data processing, writing code, and for all the knowledge, support, and encouragement that they have shared with me. A special thank you goes to Pat Evans, Barbara Mahoney, Deb Schuler, and Jeff Godfrey, for always being ready to provide assistance, organization, and oxygen.

Funding acknowledgements go to the University of Connecticut, the NOAA GOES-R and CICORE programs, and the NASA Ocean Biology and Biogeochemistry Program.

Finally, I would like to thank my family and my friends for their support and encouragement throughout the years. Parents and siblings, relatives and roommates, adventurers and dive buddies, thank you for everything.

TABLE OF CONTENTS

ABSTRACT

Seagrass ecosystems are a valuable resource, but vulnerable to changing conditions in the coastal ocean. Quantification of seagrass density and distribution from aerial imagery can be applied as a tool in resource management and ecosystem health and stability monitoring. This study investigates analytical methods for mapping eelgrass beds in an optically complex shallow, turbid estuary. Hyperspectral imagery (HSI) of Elkhorn Slough, CA was collected by the Spectroscopic Aerial Mapper with Onboard Navigation (SAMSON) instrument. *In-situ* data of water column and benthic optical properties and Hydrolight Radiative Transfer model were used to create a spectral library describing the reflectance of Elkhorn Slough at different depths with bottom coverage of seagrass or sediment. In the turbid waters of Elkhorn Slough with high levels of suspended particles, very subtle spectral differences between shallow water containing dark gray sediment or eelgrass with Leaf Area Index (LAI) up to 8 could not be accurately modeled. A second set of spectral libraries was created by selecting endmembers from the HSI data with known depth and benthic coverage ranging from sediment to dense eelgrass. Different classification algorithms were tested, and the Spectral Information Divergence algorithm was selected to compare the hyperspectral image pixels to the spectral libraries. This approach produced maps of eelgrass with 61% accuracy using 18 validation points along three transects covering sediment, sparse eelgrass (LAI=1-4), and dense eelgrass (LAI=6-8). Spectra from sediment and optically deep water in the channel were considered indistinguishable and the ancillary bathymetry was used to mask the deep channel. Eelgrass covered 10 ha of the Slough and net primary productivity totaled 1 $x10^{8}$ g C yr^{-1}. These results could not be reproduced with uncalibrated aerial photography (e.g., Google Earth). Atmospherically corrected and calibrated hyperspectral imagery was needed to resolve the subtle spectral differences between sediment and seagrass in this turbid estuary. Better calibration and atmospheric correction of the imagery

coupled with improved characterization of the inherent optical properties of the benthos and water column should lead towards the use of more radiative transfer-based approaches to mapping benthic constituents in turbid estuaries.

LIST OF FIGURES

1. Introduction

Beds of seagrasses, marine flowering plants, are among the most productive environments on earth, with the second highest economic value per hectare of any marine ecosystem (Costanza *et al.*, 1997; Waycott *et al.*, 2009). Through their physical structure, biochemical reactions in the local sediments and water column, and biomass production, seagrass beds play a major role in defining the qualities of their environment. In particular, seagrasses provide critical habitat for numerous species of fish and invertebrate and serve to stabilize sediments and protect shorelines (Gillanders 2006; Marba *et al.*, 2006). Seagrass beds only account for approximately 1% of primary production in the global ocean, yet they store about 12% of the total oceanic carbon (Smith, 1981; Hemminga and Duarte, 2000). Thus, seagrass beds are an important carbon sink for the oceans. As one of the few marine plants that is carbon limited (Invers *et al.*, 2001), they may in fact be fertilized by the addition of CO_2 into the ocean and provided with an ecological advantage in the changing climate (Palacios and Zimmerman 2007).

Seagrasses, however, are vulnerable to changes in coastal environments and have been declining worldwide (Orth *et al.*, 2006). Seagrasses are susceptible to disease, natural disasters, and anthropogenic changes such as coastal development, agricultural runoff, and pollution (Waycott *et al.*, 2009; Norse, 1993). Eutrophication of coastal waters and the associated reduction in water clarity, for example, is an increasing problem due to human population pressures along coastal regions that has already reduced seagrass distributions. The sensitivity of seagrass to light availability is so high that they may be used as an indicator species of coastal health, "coastal canaries," reacting even to small changes in water clarity (Dennison *et al.*, 1993; Tomasko *et al.*, 1996, Orth *et al.*, 2006).

Development of efficient techniques to monitor seagrass distributions and associated changes over time is vital for effective coastal management. Traditional methods for mapping seagrasses based on *in situ* surveys can become very time and labor intensive in order to obtain data with sufficient spatial and temporal resolution (Fourqurean *et al.*, 2001). In recent years, ocean color remote sensing techniques have been explored as an alternative monitoring method (Dekker *et al.*, 2005; Dierssen *et al.*, 2003; Dierssen *et al.*, 2010). Variations in benthic environments from seagrass to sediment can change the ocean color expressed at the sea surface, which can be exploited to estimate the distributions of the respective seafloor constituents. Such color changes are only visible in "optically shallow waters" where the reflectance of the seafloor contributes to the reflected light measured by a satellite or aircraft. Optically shallow conditions are primarily determined by the clarity of the water and the depth and composition of the seafloor. In turbid water, the light reflected from the bottom is attenuated rapidly within the water column and only emerges from the water column in regions with shallow bathymetry.

Many methods have been developed for conducting remote sensing of seagrasses and other benthic producers (reviewed by Kelly, 1980; Dekker *et al.*, 2006), but the approaches vary depending on the spectral resolution of available imagery. Imaging spectroscopy, measurement of the reflected light across the entire visible and near infrared spectrum, provides the opportunity to differentiate subtle differences in reflected color that are not possible from multi-channel satellite sensors. Moreover, imaging from aircraft provides data at high enough spatial resolution to map fine-scale distributions in submerged aquatic vegetation and detect potential changes in seagrass habitat due to natural and anthropogenic causes (Dierssen *et al.*, 2003; Phinn *et al.*, 2008; Dekker *et al.*, 2005; Louchard *et al.*, 2003). Many technological challenges, however, have yet to be overcome in producing calibrated imagery with sufficient signal-to-

noise for use over dark targets, such as marine environments. Unlike land surface, only a few percent of the photons that enter a water column are reflected back out again. Moreover, since most of the photons measured by an airborne sensor are scattered from atmospheric molecules and have not penetrated the water surface, atmospheric correction of the imagery is also a profound challenge (Gao *et al.*, 2007).

This study uses airborne imaging spectroscopy to map distributions of *Zostera marina,* eelgrass, and to estimate densities of the eelgrass beds. Techniques were developed and evaluated using Elkhorn Slough, California as a case study site. Freshwater inputs to the slough are associated with seasonal episodic rainfall events and can be linked to extremely high inputs of nutrients due to extensive application of fertilizer within the watershed (Chapin *et al.*, 2004). Water clarity is largely driven by the tidal cycle of the region. On the flood tide, relatively clear water from Monterey Bay enters the slough. On the ebb tide, erosion of the dark gray bottom sediment reduces the water clarity (Breaker *et al.*, 2008; Buonassissi and Dierssen, 2010). Here we show that even in this turbid estuary, hyperspectral remote sensing can be an effective tool for mapping eelgrass distributions.

2. Methods

2.1. *Data collection*

Elkhorn Slough is a 10 km long shallow tidally-forced estuary that extends nearly 5 km eastward from Monterey Bay before curving to the north (Breaker *et al.*, 2008) (Figure 1). This study focuses on approximately 2 km^2 region of Elkhorn Slough, California in the southwest near the mouth and includes Seal Bend, one of four major curves in the slough (Figure 2). Dense beds of *Z. marina*, eelgrass, occur along the northern margin of the slough in approximately 2 m water depth. In this region, the slough extends 200 m across and the main channel reaches depths of 8 m. Hyperspectral imagery (HSI) was collected on 11 September, 2006 by the Florida Environmental Research Institute (FERI) with the Spectroscopic Aerial Mapper with On-board Navigation (SAMSON) instrument (Davis *et al*., 2002). The instrument recorded data from 400 to 900 nm with approximately 3 nm resolution. The aircraft was flown at an altitude of 2800 feet above ground level, collecting data along flight swaths on a NE/SW diagonal (Figure 2) with a 1 m2 spatial resolution.

In situ measurements of the water column and benthic properties were made approximately three days earlier on September 7 and 8, 2006 at three stations in Elkhorn Slough. This study focuses on Stations 1 and 3, located approximately 100 m apart in a bed of *Zostera marina* just west of Seal Bend. Station 2 was sampled at the mouth of the Slough where it joins with Monterey Bay. The proximity to the mouth and the lack of eelgrass beds create very different water qualities at Station 2 and only Stations 1 and 3 are used in this analysis (Figure 3).

Inherent optical properties (IOPs) were measured to assess water clarity and to model the propagation of light from the eelgrass beds. The IOPs are properties of the water column that are independent of the incident light and describe the spectral distribution of light absorption and scattering in the water column. An ac-9 instrument by Wet Labs was deployed to measure the absorbance coefficient and the attenuation coefficient of the Elkhorn Slough water column. An *ac*-9 Plus package (WET Labs, Inc.) was deployed at each station in a mooring mode which sampled for six minutes at depths of 0.3 to 0.7 m below the sea surface. Salinity and temperature were measured using an SBE 19 (Sea-Bird Electronics) integrated into the sensor package. The particulate and dissolved absorption and attenuation coefficients, a_{pg} and c_{pg} were corrected for temperature, salinity and scattering effects (Aurin *et al.*, 2010). Drift offsets were obtained from a post-cruise clean water calibration. Total particulate scattering (b_p) was calculated as the difference between c_{pg} and a_{pg} assuming negligible scattering from dissolved material. Measurements of a_{pg} at 650 nm and 676 nm were used to provide a relative approximation of chlorophyll-a concentrations (Chl) in the water column (Sullivan *et al.*, 2005) such that:

The backscattering coefficient was measured with a BBFL2 (WET Labs) integrated into the sensor package. The particulate backscattering coefficient (b_{bp}) refers to all the photons that have been redirected in the backward direction due to scattering from particles in the water and, to a first order, is positively correlated to the total concentration of particles in the water (reviewed in Stramski *et al.*, 2004). Because IOPs change with the tides, sampling was done at high slack tide, the same point in the tidal cycle as when the imagery was obtained.

Divers were deployed in the water to survey the site, quantify seagrass densities if present, and collect sediment cores. Eelgrass density was measured at 5 m intervals along three 30 m

transects (Figure 3C). The locations of the start and end of each transect were recorded using GPS coordinates. Quadrats of 0.2 m^2 were placed on the bottom substrate at intervals of 5 m along the transect and shoot density was measured by counting within the quadrat. Transects were arranged in the eelgrass beds preceding Seal Bend and included areas with eelgrass and bare sediment. Including the start and end points, 7 samples were recorded along each transect for a total of 21 field validation points. Several shoots from each transect were collected and their morphometric information was measured in the lab. The height and width of the *Z. marina* leaves were measured, and used in conjunction with the shoot density to calculate the Leaf Area Index (LAI). This value is a measure of the area of eelgrass leaf (m^2) per area of bottom substrate (m^2) (Dierssen *et al.*, 2003). Reflectance of individual eelgrass leaves were measured in the laboratory using a portable FieldSpec (Analytical Spectral Devices) with an integrating sphere.

Sediment cores were collected by divers and the surface reflectance was estimated in the laboratory using the FieldSpec with the bare fiber optic probe positioned over the illuminated sample and referenced against a white spectralon plaque (99.9% reflectance) positioned similarly. Five different spectra were recorded and averaged for each core. Because of the way light refracts as it transfers through an air-water interface, these measurements approximate the spectral shape of the reflectance, but the absolute spectral magnitude may vary somewhat from the reflectance of submerged cores.

2.2. *Image analysis*

The processed imagery has a spatial resolution of ~1 m^2 and spectral resolution of approximately 3 nm, ranging from 400 nm to 900 nm. The imagery radiances were calibrated to

absolute units of W m-^{2} nm^{-1} sr^{-1} using NIST-traceable calibration standards (Kohler *et al.*, 2004). The imagery was further processed to spectral remote sensing reflectance, $R_{rs}(\lambda)$, by correcting for atmospheric and illumination effects, based on the *Tafkaa* model developed by the Naval Research Lab (Gao *et al.*, 2000; Montes and Gao, 2004). The use of *Tafkaa* in the processing of this data required a measurement of $R_{rs}(\lambda)$ at the water surface, to be matched against one of >75,000,000 solutions to find the set of atmospheric parameters that best corrected the sensor measured radiance over the same geographic point during the flight collections (Kohler 2004).

Imagery was analyzed using ENVI+IDL software by ITT Visual Information Solutions using several different spectral classification methods. Reflectance spectra from each pixel were smoothed using a Savitsky-Golay filter to remove the high frequency noise without compromising the major spectral characteristics emanating from the target. Such noise is common over dark water targets with low signal to noise (Dierssen 2011, in press). Atmospheric correction also resulted in negative reflectance values in the near infrared portion of the spectra, likely from the glint correction. Offsets of 1x10^{-3} sr^{-1} nm^{-1} and 2x10^{-3} sr^{-1} nm^{-1} were applied to the different swaths in the image to correct the spectra so that reflectance from 750 to 800 nm was null. Pixels of cloud cover and man-made objects on the water were identified by their high reflectance value in the infrared wavelengths, all pixels with reflectance higher than 4x10^{-3} sr^{-1} nm^{-1} at 799 nm (after applying the offset) were masked from the image. Water found in creeks and mudflats along Elkhorn Slough was masked by hand.

High resolution bathymetry for Elkhorn Slough was obtained by the Seafloor Mapping Lab of California State University Monterey Bay. The bathymetry data has a 0.5 m spatial resolution and presents water depth at mean lower low water (MLLW), the average of the lower low water

height of each tidal day. Imagery for this study was obtained at high slack tide with an estimated tidal height of 1.5 m and the bathymetry data were adjusted to match the tidal cycle. The shoreline was defined as areas exposed up to 0.5m at MLLW (Figure 4).

Hydrolight radiative transfer model (Sequoia Scientific) was used to solve for the expected reflectance spectra of different benthic types, creating a library of spectra describing different bottom substrates at different depths in Elkhorn Slough. Input data for Hydrolight was collected during the *in situ* sampling work and included the inherent optical properties of the water column, a Fournier-Forand phase function, benthic reflectance values, and local environmental conditions such as the day, time, wind speed, and cloud cover. The spectra in the library modeled by Hydrolight were calculated for bottom reflectance spectra of bare sediment and of eelgrass at different densities. Each bottom reflectance was modeled at depths from 1 to 5 m in 0.5 m intervals. An optically deep spectrum was also included, describing the reflectance expected from the water column alone with no influence from the benthos.

3. Results

3.1. *Benthic characterization*

Elkhorn Slough contains a deep, swift-flowing central channel flanked by wider, shallow areas where flow is restricted and sediment aggregates (Figure 4). Suitable habitat for eelgrass is limited to these shallow edges along the channel where the depths are approximately 2 m at MLLW, the average water level at the lowest tides of each tidal day. The upper limit of eelgrass extent is related to the tidal range (Palacios, 2010) which is in Elkhorn Slough is approximately 2 m above MLLW and 0.4 m below it (Elkhorn Slough Foundation). Eelgrass in Elkhorn Slough, therefore, can only be expected at depths near 2 m at MLLW, where the total water depth ranges from 1.5 m to 4 m with the tides. Anything deeper will suffer from light limitation and anything shallower is in danger of desiccation at the lowest tides.

The eelgrass beds sampled near Seal Bend were arranged as patches of mixed dense and sparse eelgrass with occasional areas of bare sediment (Figure 5). Transect 3 includes points both inside and outside of the eelgrass beds, and contains most of the bare sediment recorded in the transects. Eelgrass shoot density recorded along the transects ranged from 50 to 325 shoots m^{-2}. Each shoot contained a total of 3 to 6 leaves and an average total leaf length per shoot of 310 ±85 cm (mean ± one standard deviation). Individual leaf widths averaged 8 ± 1.4 mm and leaf heights averaged 71 ± 27 cm. Under low current flow, the eelgrass canopy averaged over 70 cm in height. When eelgrass was present, Leaf Area Index (LAI) ranged from 1.3 to 8.3 m^2 leaf m^{-2} seafloor (Figure 6). For this analysis, the seafloor was separated into three categories: dense eelgrass (LAI 6-8), sparse eelgrass (LAI 1-4), and sediment with no eelgrass ("bare" sediment, LAI=0). For simplicity we refer to stations with no eelgrass as "bare" sediment, but recognize

that the sediment may contain surface algae and biofilms. The term "sparse" eelgrass is also used here, even though most of these stations had a relatively high LAI compared to other regions. In the Bahamas Banks, for example, an LAI of greater than 2 would be considered dense (Dierssen *et al.*, 2003).

3.2. *Optical properties of eelgrass, sediment, and water column*

In order to interpret a remote sensing signal over benthic targets, the optical properties of both the seafloor and the water column must be known. Benthic reflectance measurements of sediment were obtained *in situ* within and outside the eelgrass bed (Figure 7). The spectra show dark grey sediment ranging from 3-7% reflectance across the visible spectrum. Sediment spectra increase monotonically from 400 to 700 nm and show only a slight dip at the chlorophyll absorption band at 660 nm indicating low amounts of algae associated with the sediment. Sediment within the bed is 11% darker than sediment outside the bed. The darker color of sediment is likely associated with enhanced organic detritus and other absorbing matter that become trapped within the eelgrass meadow.

Eelgrass leaf spectra obtained in the lab show low absorption in the blue and red wavelengths where chlorophyll absorbs and peak at green wavelengths (550 nm) (Figure 8). A sharp increase in reflectance is observed in the far red and infrared portion of the spectrum, the "red edge of reflectance" associated with all vegetation (Dierssen, 2006). This near infrared signal is highly absorbed by water molecules and only emerges from the water column when the benthos is very shallow. Eelgrass leaf reflectance spectra are similar to turtlegrass (Dierssen *et al.*, 2010) and other seagrass species from the literature (Stoughton, 2008; Thorhaug *et al.*, 2007). However, seagrass meadows consist of a canopy of three-dimensional leaves, as well as epiphytes, organic

debris, and sediment, that collectively contribute to the bottom reflectance. Radiative transfer within a seagrass canopy must be considered in addition to individual leaf reflectance (Zimmerman, 2003). For modeling purposes, the reflectance spectra of the eelgrass meadow were approximated as mixtures of bare sediment and eelgrass leaves.

The underwater light field is important for growth of eelgrass, which has much higher light requirements than other marine photosynthesizers (e.g. algae) (Palacios and Zimmerman, 2007). For remote sensing purposes, the water column modulates the signal reflected from the benthos. The more absorption and scattering from the water column, the less the bottom contributes to the reflected light at the sea surface. The volume of suspended particles in Elkhorn Slough, measured by the LISST, demonstrates the turbidity of Elkhorn Slough. Compared to other coastal and open ocean waters, the slough has a much higher particle load (Figure 9, Buonassissi and Dierssen, 2010). The high levels of absorbance, *a*, and attenuation, *c*, show how little light is transmitted through the water column.

Chlorophyll-a concentrations at Stations 1 and 3 estimated optically were 3.6 and 4.5 mg m^{-3}, respectively. Station 2, at the mouth of the slough, had much lower chlorophyll-a values with an average of 0.8 mg m^{-3}. Overall, the IOP data show that Elkhorn Slough is a very turbid estuary with little light penetration and high concentrations of scattering and absorbing suspended particles.

Along with the water depth, the optical characteristics of the seafloor and the water column both play a major role in determining the Remote Sensing Reflectance (R_{rs}, the water-leaving radiance normalized to the incident downwelling irradiance). Spectra from over eelgrass show lower magnitudes and broader peaks than spectra from over sediment or deep water. Deep water

and sediment are quite similar to one another, with very close magnitudes and peaks, although the average deep water spectrum has a steeper slope and more blue absorption than sediment (Figure 11). Standard error bars from sediment and deep water samples overlap one another across the entire spectrum, indicating that the difference between deep water and sediment spectra from Elkhorn Slough is not significant ($p>0.05$) (Figure 12).

3.3. *Development of spectral library*

Various methods have been used to map benthic features from remote sensing reflectance from strictly empirical to semi-analytical. The approach for classifying the image into selected categories was to first develop a spectral library or look-up table of R_{rs} found over the different targets and then apply an algorithm to best match each spectrum from the imagery to those in the spectral library. First a radiometric approach was used to develop the spectral library from knowledge of optical properties of the benthos and water column. The library included an optically deep spectrum and spectra from depths between 0.5 and 5 m in 0.5 m-intervals of sediment and eelgrass. This depth range was selected to include slightly more than the full range of expected eelgrass depths over the tidal cycle. Modeling showed that the water became optically deep at 3.5 m depth where the bottom no longer contributed to the signal observed at the sea surface and the spectra become indistinguishable from deep water (Figure 10). The modeled spectra were able to reproduce some of the features present in the HSI, but the differences between eelgrass and sediment were not well reproduced. For example, the HSI peaks at 560 nm for sediment while the Hydrolight spectra peak at 585 nm. The HSI also has a much rounder shape across the green wavelengths for eelgrass spectra than was reproduced by the model. In addition, the magnitude of the spectra was higher in the green portions of the spectrum. Better agreement or "closure" was not achieved between the modeled and measured

spectra by changing the model inputs (e.g., phase functions) or applying atmospheric correction offsets to the imagery (Louchard *et al.*, 2003) and an alternate approach was used to make the spectral library.

Spectral libraries can also be developed by using the spectral reflectance of known targets or "endmembers" within the imagery. Such an approach compensates for any problems with calibration or atmospheric correction of the imagery, but requires prior knowledge of pixels within an image. Since the benthic targets were restricted to a limited depth range (2-3 m) in this study, a simple spectral library was constructed from three known pixels in the imagery corresponding to eelgrass and sediment at 2 m. Specifically, the selected points had LAI values of 0, 3.2, and 7.0 describing sediment, sparse eelgrass, and dense eelgrass. With 3 points reserved for model formulation, 18 points remained for field validation. The spectral library including these three points is referred to as the shallow *in situ*-image matchup library. A second library, the deep *in situ*-image matchup library, includes the same three points from the shallow library as well as a spectra describing optically deep water. The optically deep spectrum was taken from a randomly selected location in the deep channel of Elkhorn Slough and is representative of the mean deep water spectrum (Figure 11).

3.4. *Image Classification*

Various statistical approaches can be used to match spectra from the HSI to the spectral library. Some methods are more sensitive to differences in spectral shape (i.e., dips and peaks in the spectra) and others to spectral magnitude (i.e., how light or dark the entire spectrum is). The results from four different classification algorithms (Canty, 2007; Research Systems Inc., 2003) were compared in terms of their accuracy at predicting the 18 validation points. The

parallelepiped did not classify any of the validation points and both the binary encoding algorithm and spectral angle mapper approaches accurately classified only 28% of the points. Two models outperformed all others with over 60% of the validation points properly classified: spectral information divergence (SID) with 61% (11/18) and the minimum distance algorithm with 67% (12/18). Of these two models, the SID was considered best because it was able to correctly classify the shallow habitat surrounding the eelgrass meadows as sediment (Figure 13A). The minimum distance algorithm modeled 85% of the total benthic area of the slough as sparse eelgrass, which is not consistent with observations during the sampling time, with the known depth limits of eelgrass in Elkhorn slough, or with descriptions of eelgrass distribution in Elkhorn Slough from other studies (Palacios 2010; Palacios and Zimmerman 2007).

As mentioned earlier, the spectra from sediment and optically deep water in the channel were considered indistinguishable (Figure 11). This result was further demonstrated by adding a deep water spectra to the spectral library. The SID classification was still able to map the locations of the beds, but the deep water channel was indistinguishable from shallow sediment habitat and classification of these two endmembers was confused throughout the image (Figure 13B). Twenty-five percent of the shallow water area was classified as deep water, and 39% of the deep water was classified as either sediment or eelgrass. Hence, to produce the best habitat map for the Elkhorn Slough, deep water in the channel was masked using the high resolution bathymetry for the Slough.

A classification accuracy matrix was constructed to analyze the types of errors most common to the classification approach. If the classification was perfect, numbers would be found only along the diagonal where the measured and modeled categories match. The matrix also shows errors of omission when the classification failed to include a pixel in a category and errors of

commission when the model added a pixel to a category. The largest source of error was in classifying sparse eelgrass as dense. Overall, 100% of the dense eelgrass was correctly located, 29% of the sparse eelgrass, and 67% of the sediment.

After masking land, cloud, and deep water from the HSI data, the resulting habitat map reproduced the known features of this portion of Elkhorn Slough. Within the image extent, there was approximately 0.2 km² of optically deep water (>3.5 m) and 0.2 km² of optically shallow water considered potential eelgrass habitat. A small eelgrass bed was located before Seal Bend where the validation points were located and a large eelgrass bed was also mapped across the northern curve of Seal Bend. This second bed shows a two-pronged shape through the eastern side of the bend that has been previously mapped in Elkhorn Slough (Zimmerman, 2006). Most of the points classified as eelgrass are included in these two eelgrass beds, but a few small areas were also classified as sparse or dense eelgrass. Along the southern edge of Elkhorn Slough, east of Seal Bend, there is a long patch following the shoreline classified as sparse eelgrass. The northern edge of Seal Bend shows a long, thin line of points classified as sparse and dense eelgrass along the shoreline. A patch of clouds obscures part of the far western end of the image, but much of the shallow water in that region was classified as containing eelgrass. The presence or absence of eelgrass in these regions is not known.

4. Discussion

Remote sensing of vegetation in coastal waters presents unique challenges relative to terrestrial systems. In the absence of an overlying water column, the normalized difference vegetation index (NDVI), a ratio of the near infrared and visible bands, can be effectively used to detect green biomass (Campbell 1996). In oceanic waters, however, the infrared portion of the spectrum is highly absorbed by the water column and algorithms are generally restricted to the visible spectrum (400-700 nm). Moreover, the optical signal coming from the benthic vegetation is strongly modulated by the effects of the overlying water column. Remote sensing reflectance in optically shallow water must be evaluated in the context of the water depth and inherent optical properties of the water column. In this study conducted in Elkhorn Slough, a highly absorbing water column returned a low remote sensing reflectance signal near the detection limits of current technology. The submerged sediment in Elkhorn Slough was dark grey in color, distinguishable from eelgrass only by subtle spectral differences. Unlike regions with clear water and bright sand (e.g., Bahamas), this was a challenging marine environment in which to test the applicability and limits of hyperspectral remote sensing. Below, we discuss the challenges inherent to the classification approach, use of the imagery to quantify eelgrass productivity, and the benefits of hyperspectral imagery compared to uncalibrated aerial photography.

4.1. *Classification approach*

Many methods are possible for mapping seagrass distributions from ocean color imagery (Dekker *et al.*, 2005). The most portable and robust methods are based on radiative transfer theory where the reflectance of the bottom is considered in the context of the absorbing and

scattering properties of the water column (Lee *et al.*, 1999; Dierssen *et al.*, 2003). Here, we developed a spectral library using a radiative transfer model to propagate bottom-reflected light through different depths of water column for our measured water column optical properties (Louchard *et al.*, 2003; Mobley *et al.*, 2005). However, modeled remote sensing reflectance did not accurately match the reflectance from the imagery for known sediment and seagrass targets for application of this approach. Discrepancies were observed in both shape and magnitude of the spectral reflectance (Figure 15).

Our inability to obtain closure between the model and imagery in this study may be due to a number of factors. Elkhorn Slough is a dark, turbid, and complex body of water with high concentrations of absorbing particle that change with the tidal cycles. Due to field constraints, the water column sampling occurred a few days prior to the overflight and optical properties in the water may have changed from those used in the model. Secondly, the IOP data was not hyperspectral and was only provided at nine wavelengths throughout the visible spectrum. The degraded spectral resolution showed less variability between sediment and sand from the model than the imagery, and the peaks in the spectra were shifted to coincide with the nine wavelengths sampled with the instrumentation. Third, the field of view of a benthic spectrometer is small (cm-scale) and the resulting benthic reflectance measurements used in the model may not be representative of the diverse substrate within a pixel (m-scale). Finally, atmospheric correction presents challenges in coastal waters and variability in assumptions about aerosols can lead to errors in the retrieved reflectances from the imagery (Dierssen and Randolph, 2011) that would make them different from an idealized model. Often adjustments or spectral offsets are made to the image-derived reflectance values to account for atmospheric correction problems and to more closely match the spectral library (Louchard *et al.*, 2003; Dierssen *et al.*, 2009; Mobley *et al.*,

2005) and such a correction was employed here to increase the negative reflectances in the near infrared.

Because of the difficulty in accurately modeling the reflectance spectra, the spectral library was constructed by selecting endmembers of known points within the HSI. Such classification approaches are commonly used for identifying features within an image and do not require precise calibration and atmospheric correction of the imagery (Lu and Weng, 2007; Song *et al.*, 2001; Kawata *et al.*, 1990). A major disadvantage of this type of approach is that pixels with each desired bottom type at each desired bottom depth must be known and identified *a priori* within each image. The approach cannot map unknown features or areas with the same substrate but at different depths from known pixels in the imagery. Such methods also do not provide mathematical algorithms that can be extrapolated to other images and regions. Here, eelgrass was found only in a limited depth range of >2 meters at MLLW due to light availability (Zimmerman and Caffrey, 2002; Zimmerman *et al.*, 1994) and only three endmembers were needed to construct the library.

In this study, the spectral information divergence (SID) was found to best match the reflectance spectra from each pixel to the spectral library, as well as preserve the general features of the habitat. . Where measures such as the spectral angle mapper, Euclidean distance measure, and spectral correlation measure use measurements of angles, distances, and vector cross-correlations between the known reference spectra and the unknown, SID measures discrepancies of probability distributions between them. In a comparison study testing discrimination of terrestrial ground cover, SID was found to be 3 to 4 times more effective at spectral discrimination than other methods, including the spectral angle mapper (Chang 2000). Additionally, the SID algorithm also returned better results than the spectral correlation measure,

which was shown to be extremely sensitive to noise in the signal (Van der Meer, 2006). Based on the spectral information measure, introduced in 2000, the SID was specifically designed for hyperspectral datasets. The method is better able to account for mixed pixels, made up of a combination of materials with different spectral signatures, and for variation in the signal due to atmospheric effects (Chang, 1999; Chang 2000).

Water surfaces are three-dimensional and contain capillary and gravity waves that reflect skylight in different directions. Removing the contribution of skylight to the remotely sensed reflectance is a challenging problem, especially when imagery is obtained at different angles with respect to the sun. Gould *et al.* (2001) demonstrate that without appropriate skylight correction, measurements will be significantly higher than the true reflectance value, particularly in the blue range of the spectrum (400-500 nm). The problems with skylight corrections are evident in the HSI data along the juncture between the different flight swaths (Figure 16). The spectra along the edges of each swath show increased reflectance in blue wavelengths compared to the other swaths of imagery. To prevent misclassification, a smaller range of the available wavebands from 500 nm to 800 nm was used in the SID spectral classification algorithm. This portion of the spectra removed both the errors in the blue and the calibration errors in the infrared, as discussed previously. The primary spectral differences between sediment and eelgrass reflectance can be seen in this range (see Figure 11).

The accuracy assessment matrix showed that the majority of validation data points (61%) were successfully classified into sediment, sparse, and dense eelgrass. The most common classification error was an error of omission, counting areas of sparse eelgrass as sediment. Errors in the classification could be due to problems with the classification algorithm or in the validation dataset itself. Since GPS does not work underwater, only the start and the end of the

transects were marked by GPS at the sea surface. Points measured in between the 30 m transects were calculated assuming an equal distance between all points on the line, and may not be exactly correct. Also, the quadrat used to calculate the LAI of each location was only 0.2 m^2, smaller than the 1 m^2 pixels in the HSI and may not be representative of the entire image pixel.

4.2. *Quantitative estimates of productivity*

Qualitative modeling of eelgrass distributions (sparse, dense, and sediment) is useful for assessing habitats for environmental monitoring purposes. Maps produced here, for example, may be considered as a baseline for future studies monitoring changes in the Elkhorn Slough environment and assessing the maximum depth of occurrence. As a light-limited plant, the depth of eelgrass can be an indicator of water quality (Dennison *et al.*, 1993; Orth *et al.*, 2006). However, quantitative measures, such as leaf area index (LAI), are necessary for extrapolation to biogeochemical processes including system productivity and carbon flux. Leaf area index represents the leaf area exposed to the light field can be directly related to the amount of photosynthesis in the seagrass bed. Furthermore, the field data required to estimate LAI (e.g., leaf length and width, shoot density) provide ancillary information on the morphology of the canopy that can be useful when considering spectral signatures derived under varying physical conditions (e.g., tidal flow) or from different regions. For example, canopy height and shoot density are essential for modeling the photon flux within the canopy and for considering effects of flow on canopy architecture and light fields (Zimmerman 2003; Hedley and Enriquez, 2010). Moreover, regions with sparse, long shoots might have different relationships between bottom reflectance and LAI than regions with short, dense shoots.

The qualitative categories used in this analysis can be related directly to LAI and net primary productivity using some simple empirical relationships. LAI can be used to obtain an estimate of total organic carbon by using it to estimate the fresh weight and dry weight of seagrass (van Tussenbroek, 1998; Sfriso and Ghetti, 1998), which is then related to the total organic carbon (Hemminga and Duarte, 2000). Elkhorn Slough is highly seasonal, with variable growth rates throughout the year. Palacios and Zimmerman (2007) showed that growth rates of eelgrass in Elkhorn Slough vary from 1-3%, depending on season and light availability. Assuming a growth rate of 2%, the net primary productivity (NPP) of eelgrass in Elkhorn Slough can be estimated from the distributions of eelgrass mapped here. With an average LAI of 2.6 in the sparse eelgrass (4.845 ha) and 7.4 in the dense eelgrass (5.148 ha), this gives a rate of 7 g C m^{-2} d^{-1} and a total NPP of 1 x10^{8} g C yr^{-1} in Elkhorn Slough, or 100 tons C yr^{-1}.

Quantification of NPP can be useful in developing ecosystem carbon budgets and further assessments of the contribution of shallow water ecosystems to global biogeochemistry. With growing concern over atmospheric CO_2 levels, the role of seagrasses in the carbon cycles warrants further exploration from small (Palacios and Zimmerman, 2007) to regional scales (Dierssen *et al.*, 2010). The precise fate of the carbon fixed in this system is not well constrained, but some carbon will be exported offshore, some invested in the bed and root structure, and some will be grazed upon and moved to the next trophic level.

4.3. *Benefits of hyperspectral imagery versus aerial photography*

While useful in both habitat and biogeochemical studies, obtaining and processing hyperspectral imagery is costly and can be time and labor intensive. An environmental decision maker may question whether eelgrass distributions could be accurately mapped with uncalibrated

images either from satellites or aircraft. Over the past two decades, several aerial images have been recorded over Elkhorn Slough. The earliest images are black and white and the more recent are in color with each pixel composed of 3 wavebands: a red, a green, and a blue (RGB). In some of these images, differences can be seen in the water color in the areas known to contain eelgrass and such color changes may be useful in mapping eelgrass. Depending on the level of accuracy needed in the distributions, simple RGB imagery may provide eelgrass maps without the need for hyperspectral data.

Google Earth's historical imagery data has one clear image of Elkhorn Slough from 2006, recorded on 25 May 2006 by Digital Globe (Figure 17). This striking image clearly shows dark eelgrass located centrally in Seal Bend and a lighter bed to the west. With prior knowledge of eelgrass in these regions, a drafter could outline the extent of the beds from the RGB imagery. The human eye is very good at classification of light and dark features (Dierssen *et al.*, 2006), but surprisingly these eelgrass beds cannot be easily defined and classified with image analysis techniques. The image was analyzed using both unsupervised classification techniques and with a supervised classification using a spectral library created from known locations of eelgrass and sediment. While Google Earth imagery is able to locate the general area of eelgrass beds, the resulting information on distribution and density of submerged vegetation does not match the quality of the hyperspectral imagery (Figure 18, Figure 19). In all three classifications, the patchiness of the eelgrass beds in Elkhorn Slough is not evident, and no clear and consistent edge to the eelgrass beds is delineated. The greatest difficulty was in locating the eelgrass beds to the west of Seal Bend near the sampling stations. In Figure 18, for example, the eelgrass to the west is considered the same as sediment located around the central bed in both classifications (green targets). To your eye, the bed in the west appears dark, but the actual intensity is similar to

sediment around the central bed. Such challenges in photointerpretation require considerable knowledge form the analyst both in terms of determining what is eelgrass and where assigning appropriate boundaries to the beds.

The imagery in Google Earth appears to have been collected without regard to the solar zenith angle or the sensor viewing angle, both of which ought to be taken into consideration when collecting aerial imagery for ocean color remote sensing. The image shows cross-track illumination with average reflectance magnitudes that increase from east to west. This increased brightness overwhelms the dark signal of eelgrass in the west, and sediment in the east is darkened in comparison.

For ocean applications, patching together images collected at different sensor angles, solar zenith angles, and sky conditions, a common practice for uncalibrated aerial photographs, can result in vastly different retrievals of eelgrass. Atmospherically corrected imagery requires a range of wavelengths that are not available in RGB imagery. The noticeable and uneven glint and skylight in the Google Earth imagery make both unsupervised and supervised approaches challenging, particularly given the limited spectral data. Sun glint also plagues the HSI and can interfere with classification approaches, but atmospheric correction routines are being actively developed to remove glint (Hedley *et al.*, 2005).

The hyperspectral analysis conducted here showed very subtle spectral differences between eelgrass and sediment that would not be evident in RGB imagery. With only 3 broad wavebands to define the spectral shape, very similar R:G:B ratios are produced for all of Elkhorn Slough. Unable to use spectral shape, the classification algorithms rely instead on differences in the magnitude or intensity of the reflected light. Unevenly illuminated images result in maps that

show more eelgrass than is actually present in the darker eastern side of the image, and less than is present in the brighter areas to the west. While the aerial photography can have some utility in regions with known benthos, considerable prior knowledge is required to interpret where the beds are located, their boundaries, and to determine eelgrass density from only the intensity of the signal rather than the spectral shape..

4.4. *Conclusion*

Here we have shown that airborne remote sensing can be successfully used to map eelgrass distributions, even in the dark turbid waters of Elkhorn Slough. Hyperspectral imagery was required in order to resolve subtle shifts in reflected color and is vital for the future of coastal ocean remote sensing. Sensors need to be designed to handle the wide range of reflectances between dark, absorbing water and bright reflective sediment and have the spectral resolution necessary to deduce subtle spectral differences (Mouroulis *et al.*, 2008; Corson *et al*., 2008). The high spectral resolution allows for quantification of submerged aquatic vegetation and to account for coastal vegetation in biogeochemical investigations. Improvements in calibration and atmospheric correction will further increase the utility of these tools for monitoring and managing coastal resources through environmental changes, both natural and anthropogenic, and lead to improved analysis techniques that are radiometrically-based and can be universally applied without considerable *a priori* knowledge. Such improvements will help in mapping of vulnerable coastal habitats and assessing responses to physical disturbances and changes in water temperatures, water clarity, nutrient levels, and atmospheric CO_2 concentrations.

References

Aurin D, Dierssen HM, Twardowski MS, Roesler CS (2010) Optical complexity in Long Island Sound and implications for coastal ocean color remote sensing. Journal of Geophysical Research 115

Breaker LC, Broenkow WW, Watson WE, Jo Y-H (2008) Tidal and nontidal oscillations in Elkhorn Slough, CA. Estuaries and Coasts 31:239-257

Buonassissi CJ, Dierssen HM (2010) A regional comparison of particle size distributions and the power law approximation in oceanic and estuarine surface waters. Journal of Geophysical Research 115

Campbell JB (1996) Introduction to Remote Sensing, Vol. The Guilford Press, New York

Canty MJ (2007) Image analysis, classification, and change detection in remote sensing: with algorithms for ENVI/IDL, Vol. CRC Press

Chang C-I (1999) Spectral Information Divergence for Hyperspectral Image Analysis Geoscience and Remote Sensing Symposium. IEEE, p 509-511

Corson MR, Korwan DR, Lucke RL, Snyder WA, Davis CO (2008) The Hyperspectral Imagery for the Coastal Ocean (HICO) on the International Space Station. Geoscience and Remote Sensing Sympsoium, IGARSS 2008, IEEE International, Vol IV-101

Costanza R, d'Arge R, de Groot R, Farber S, Grasso M, Hannon B, Limburg K, Naeem S, O'Neill RV, Paruelo J, Raskin RG, Sutton P, van den Belt M (1997) The value of the world's ecosystem services and natural capital. Nature 387:253

Davis CO, Bowles J, Leathers RA, Korwan D, Downes TV, Snyder WA, Rhea WJ, Chen W, Fisher J, Bissett WP, and others (2002) Ocean PHILLS hyperspectral imager: design, characterization, and calibration. Optics Express 10:210-221

Dekker AG, Brando VE, Anstee JM (2005) Retrospective seagrass change detection in a shallow coastal tidal Australian lake. Remote Sensing of Environment 97:415-433

Dennison WC, Orth RJ, Moore KA, Stevenson JC, Carter V, Kollar S, Bergstrom PW, Batiuk RA (1993) Assessing water quality with submersed aquatic vegetation. BioScience 43:86-94

Dierssen HM, Randolph K (2011 (in press)) Remote Sensing of Ocean Color. In: Meyers RA (ed) Encyclopedia of Sustainability Science and Technology. Springer-Verlag

Dierssen HM, Zimmerman RC, Burdige DJ (2009) Optics and remote sensing of Bahamian carbonate sediment whitings and potential relationship to wind-driven Langmuir circulation. Biogeosciences 6:487-500

Dierssen HM, Zimmerman RC, Drake LA, Burdige D (2010) Benthic ecology from space: optics and net primary production across the Great Bahama Bank from seagrass and benthic algae. Marine Ecology Progress Series 411:1-15

Dierssen HM, Zimmerman RC, Leathers RA, Downes TV, Davis CO (2003) Ocean color remote sensing of seagrass and bathymetry in the Bahamas Banks by high-resolution airborne imagery. Limnology and Oceanography 48:444-455

Fourqurean JW, Willsie A, Rose CD, Rutten LM (2001) Spatial and temporal pattern in seagrass community composition and productivity in south Florida. Marine Biology 138:341-354

Gao B-C, Montes MJ, Ahmad Z, Davis CO (2000) Atmospheric correction algorithm for hyperspectral remote sensing of ocean color from space. Applied Optics 39:887-896

Gao B-C, Montes MJ, Davis CO (2004) Refinement of wavelength calibrations of hyperspectral imaging data using a spectrum-matching technique. Remote Sensing of Environment 90:424-433

Gao B-C, Montes MJ, Li R-R, Dierssen HM, Davis CO (2007) An atmospheric correction algorithm for remote sensing of bright coastal waters using MODIS land and ocean channels in the solar spectral region. IEEE Transactions on Geoscience and Remote Sensing 45:1835-1843

Gould RW, Arnone RA, Sydor M (2001) Absorption, Scattering, and Remote-Sensing Reflectance Relationships in Coastal Waters: Testing a New Inversion Algorithm. Journal of Coastal Research 17:328-341

Hedley JD, Harborne A, Mumby P (2005) Technical note: simple and robust removal of sun glint for mapping shallow water benthos. International Journal of Remote Sensing 26:2107-2112

Hedley J, Enriquez S (2010) Optical properties of canopies of the tropical seagrass *Thalassia testudinum* estimated by a three-dimensional radiative transfer model. Limnology and Oceanography 55:1537-1550

Hemminga MA, Duarte CM (2000) Seagrass Ecology, Vol. Cambridge University Press

Invers O, Zimmerman RC, Alberte RS, Perez M, Romero J (2001) Inorganic carbon sources for seagrass photosynthesis: an experimental evaluation of bicarbonate use in species inhabiting temperate waters. Journal of Experimental Marine Biology and Ecology 265:203-217

Kawata Y, Ohtani A, Kusaka T, Ueno S (1990) Classification accuracy for the MOS-1 MESSR data before and after the atmospheric correction. IEEE Transactions on Geoscience and Remote Sensing 28:755-760

Kohler DDR, Bissett WP, Steward RG, Davis CO (2004) New approach for the radiometric calibration of spectral imaging systems. Optics Express 12

Lee Z, Carder KL, Mobley CD, Steward RG, Patch JS (1999) Hyperspectral remote sensing for shallow waters: Deriving bottom depths and water properties by optimization. Applied Optics 38:3831-3843

Louchard EM, Reid RP, Stephens FC, Davis CO, Leathers RA, Downes TV (2003) Optical remote sensing of benthic habitats and bathymetry in coastal environments at Lee Stocking Island, Bahamas: A comparative spectral classification approach. Limnology and Oceanography 48:511-521

Lu D, Weng Q (2007) A survey of image classification methods and techniques for improving classification performance. International Journal of Remote Sensing 28:823-870

Marbà N, Holmer M, Gacia E, Barron C (2006) Seagrass Beds and Coastal Biogeochemistry. In: Larkum AWD, Orth RJ, Duarte CM (eds) Seagrasses: Biology, Ecology and Conservation. Springer

Mobley CD, Sundman LK, Davis CO, Bowles JH, Downes TV, Leathers RA, Montes MJ, Bissett WP, Kohler DDR, Reid RP, Louchard EM, Gleason A (2005) Interpretation of hyperspectral remote-sensing imagery by spectrum matching and look-up tables. Applied Optics 44:3576-3592

Mouroulis P, Green RO, Wilson DW (2008) Optical design of a coastal ocean imaging spectrometer. Optics Express 16:9087-9096

Norse EA (1993) Global marine Biological Diversity: A Strategy for Building Conservation into Decision Making, Vol

Orth RJ, Carruthers TJB, Dennison WC, Duarte CM, Fourqurean JW, Heck KL, Hughes AR, Kendrick GA, Kenworthy WJ, Olyarnik S, Short FT, Waycott M, Williams SL (2006) A Global Crisis for Seagrass Ecosystems. BioScience 56:987-996

Palacios S (2010) Eelgrass: factors that control distribution and abundance in Pacific Coast estuaries and a case study of Elkhorn Slough, California

Palacios SL, Zimmerman RC (2007) Response of eelgrass Zostera marina to CO2 enrichment: possible impacts of climate change and potential for remediation of coastal habitats. Marine Ecology Progress Series 344:1-13

Research Systems I (2003) ENVI user's guide, Vol. Research Systems

Sfriso A, Ghetti PF (1998) Seasonal variation in biomass, morphometric parameters and production of seagrass in the lagoon of Venice. Aquatic Botany 61:207-223

Smith SV (1981) Marine Macrophytes as a Global Carbon Sink. Science 211:838-840

Song C, Woodcock CE, Seto KC, Lenney MP, Macomber SA (2001) Classification and change detection using Landsat TM data: When and how to correct atmospheric effects? Remote Sensing of Environment 75:230-244

Tomasko DA, Dawes CJ, Hall MO (1996) The effects of anthropogenic nutrient enrichment on turtle grass (Thalassia testudinum) in Sarasota Bay, Florida. Estuaries 19:448-456

Van der Meer F (2006) The effectiveness of spectral similarity measures for the analysis of hyperspectral imagery. International Journal of Applied Earth Observation and Geoinformation 8:3-17

van Tussenbroek BI (1998) Above- and below-ground biomass and production by Thalassia testudinum in a tropical reef lagoon. Aquatic Botany 61:62-82

Waycott M, Duarte CM, Carruthers TJB, Orth RJ, Dennison WC, Olyarnik S, Calladine A, Fourqurean JW, Heck KL, Hughes AR, Kendrick GA, Kenworthy WJ, Short FT, Williams SL (2009) Accelerating loss of seagrasses across the globe threatens coastal ecosystems. Proceedings of the National Academy of Sciences of the United States of America 106:12377-12381

Zimmerman RC (2003) A biooptical model of irradiance distribution and photosynthesis in seagrass canopies. Limnology and Oceanography 48:568-585

Zimmerman RC (2006) Light and photosynthesis in seagrass meadows. In: Larkum AWD, Duarte CM, Orth RJ (eds) Seagrasses: Biology, Ecology and Conservation. Springer, p 303-321

Zimmerman RC, Cabello-Pasini A, Alberte RS (1994) Modeling daily production of aquatic macrophytes from irradiance measurements: a comparative analysis. Marine Ecology Progress Series 114:185-196

Zimmerman RC, Caffrey J (2002) Primary Producers. In: Changes in a California estuary: a profile of Elkhorn Slough. Elkhorn Slough Foundation, p 118-133

Figure Legends

Figure 1 Map of California and the location of Elkhorn Slough

This study was conducted in Elkhorn Slough located along the California coastline at the head of Monterey Bay.

Figure 2 Hyperspectral image

A pseudo true color representation of the hyperspectral imagery data of a portion of Elkhorn Slough, CA recorded by the SAMSON instrument on 11 Sept, 2006

Figure 3 Map of Elkhorn Slough *in situ* sample locations

A) Sampling stations were situated at the mouth of Elkhorn Slough (Station 2) and near Seal Bend (Stations 1 and 3).

B) Field data were collected primarily to the west of Seal Bend.

C) Three transects measuring eelgrass density were collected by divers and include the 18 validation points used in the study.

Figure 4 Bathymetry of Elkhorn Slough

Bathymetry of Elkhorn Slough at the time of image collection corresponding to high slack tide. Suitable habitat for eelgrass includes depths from -1 to -3.5 m, including the red, orange, and light green areas of the map. A deep channel (deeper than -5.5 m) runs through the center of Elkhorn Slough with higher current flow and no eelgrass.

Figure 5 Leaf Area Index along transects

The distribution of eelgrass Leaf Area Index (LAI) measured along the three transects shows a patchy distribution with considerable variability between dense eelgrass (LAI=6-8), sparse eelgrass (LAI=1-4), and sediment (LAI=0).

Figure 6 Frequency histogram of Leaf Area Index

The number of field stations containing eelgrass with Leaf Area Indices ranging from dense (6-8) to sparse (1-4) to sediment (0).

Figure 7 DiveSpec reflectance spectra

Reflectance of sediment measured by divers both within and outside the eelgrass beds.

Figure 8 Reflectance of eelgrass leaf and sediment core

Reflectance spectra were measured in the laboratory from a sediment core and an eelgrass leaf.

Figure 9 Particle size distributions in Elkhorn Slough compared to other bodies of water

Measurements of particle size distributions (particle diameter versus concentration) from water collected throughout the world. The particle concentrations from Elkhorn Slough are higher than other estuaries, including Long Island Sound, indicating a very turbid particle-laden water body.

Figure 10 Remote sensing reflectance modeled for different bottom types

Remote sensing reflectance (sr^{-1}) modeled with measured water column properties and different types of seafloor constituents. Three lines are shown for sediment and eelgrass corresponding to different water depths of 1 m (top line), 2 m (middle line), and 3 m (bottom line). The modeled spectrum for deep water, shown in black, is indistinguishable from eelgrass or sediment at 4 m depth.

Figure 11 Spectral library of image-based endmembers

Remote sensing reflectance (sr^{-1}) from the hyperspectral imagery was used to create a spectral library. The selected endmembers include dense eelgrass (LAI = 7.0), sparse eelgrass (LAI = 3.2), and bare sediment all at approximately 2 m depth. A spectrum describing deep water was taken from the deep channel at a depth of 6.5 m.

Figure 12 Standard errors in sediment and deep water spectra

The average remote sensing reflectance (sr^{-1}) spectrum with one standard error for all field stations containing bare sediment on the seafloor (<3 m water depth) compared to a similar number of deep water (>5.5 m water depth) pixels. The overlap of error bars across the visible spectrum indicate no significant difference between two spectra and show that deep water and sediment cannot be spectrally distinguished.

Figure 13 Eelgrass classification from the hyperspectral imagery

A) Eelgrass was mapped from the hyperspectral imagery using the spectral information divergence classification algorithm and a spectral library with image-based endmembers with the deep channel masked in black.

B) Without masking the deep water, the classification approach can map the eelgrass beds but cannot distinguish bare sediment (yellow) from deep water (brown).

Figure 14 Classification accuracy matrix

Accuracy matrix of the classification shown in Figure 13A for the 18 validation data points ranging from dense eelgrass to bare sediment. The boxes in red indicate agreement between the image classification and the validation data points of 61% (11/18). All five of the locations with dense eelgrass were correctly located, and four of the six locations with sediment. Sparse eelgrass was only classified with 29% accuracy.

Figure 15 Comparison of spectra from the hyperspectral imagery and radiative transfer model

Remote sensing reflectance (sr^{-1}) for stations containing eelgrass and sediment bottoms from the radiative transfer model (dotted lines) were higher in magnitude than the spectra from the hyperspectral image (solid lines).

Figure 16 Glint visible in the hyperspectral imagery

A pseudo true color image of the study location from the SAMSON imagery shows differences in the magnitude of reflected light due to sun glint between the NE/SW flight track lines (arrows).

Figure 17 Historical imagery from Google Earth

An aerial photograph or image of Elkhorn Slough, CA taken 25 May 2006 by Digital Globe available in the Google Earth archive.

Figure 18 Results of unsupervised classification of Google Earth imagery

Both unsupervised classification algorithms show the general shape of the main eelgrass bed in the central Seal Bend, but classify eelgrass in the smaller bed to the west in the same class as sediment in the central bed (green).

Figure 19 Results of supervised classification of Google Earth imagery

The presence and absence of eelgrass appears appropriately classified in the eelgrass bed in Seal Bend, but the smaller bed in the western part of the Slough is significantly smaller than expected.

Figures

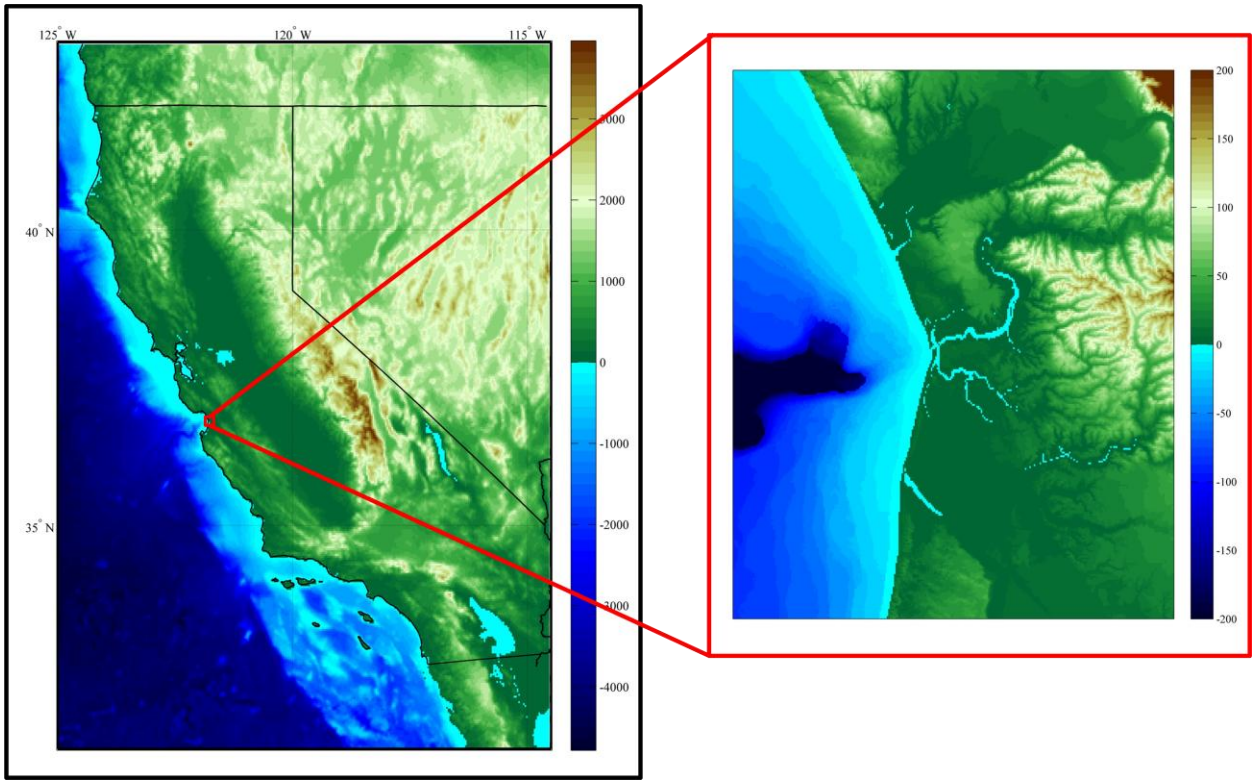

Figure 1 Map of California and the location of Elkhorn Slough

This study was conducted in Elkhorn Slough located along the California coastline at the head of Monterey Bay.

Figure 2 Hyperspectral image

A pseudo true color representation of the hyperspectral imagery data of a portion of Elkhorn Slough, CA recorded by the SAMSON instrument on 11 Sept, 2006

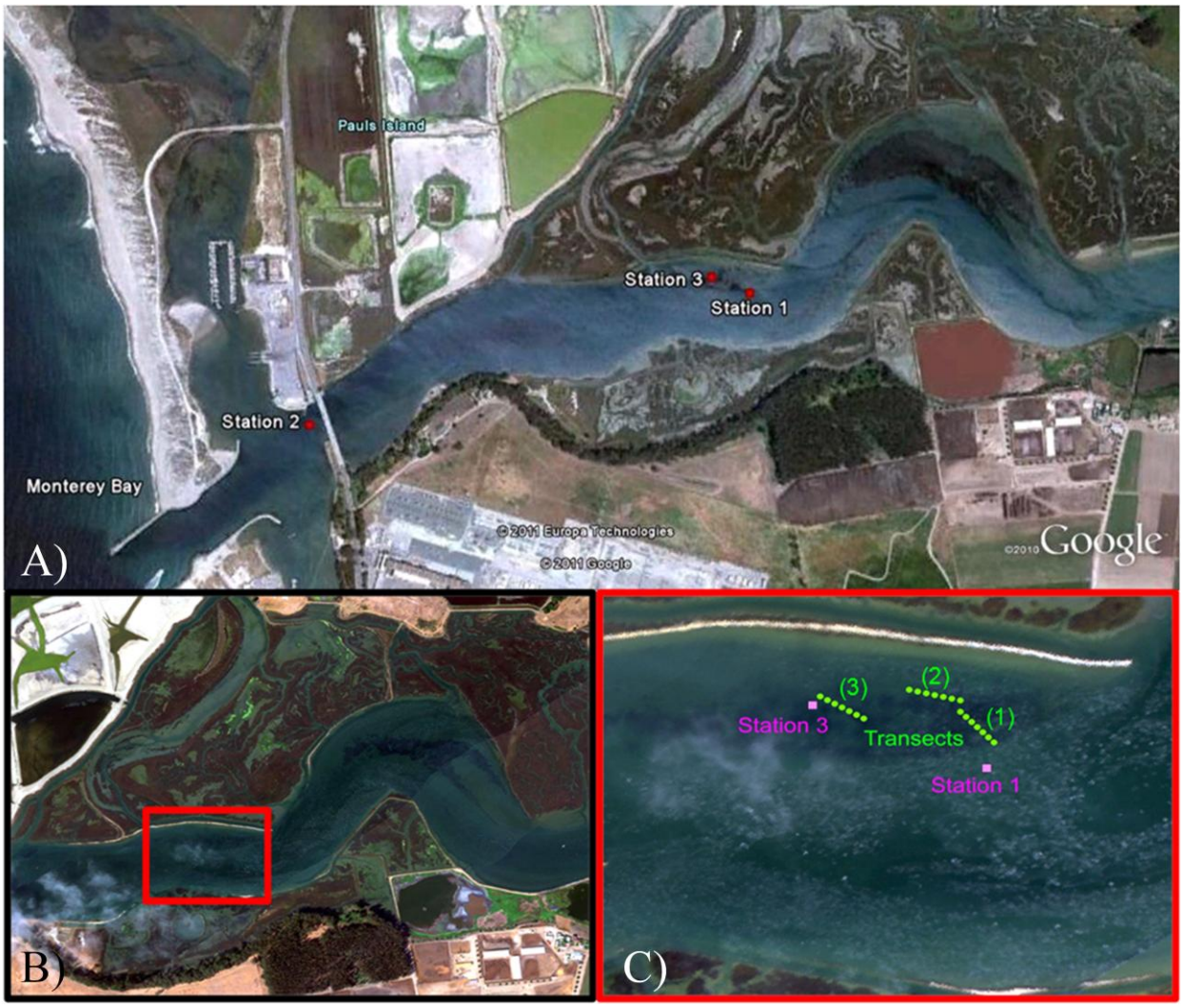

Figure 3 Map of Elkhorn Slough *in situ* sample locations

A) Sampling stations were situated at the mouth of Elkhorn Slough (Station 2) and near Seal Bend (Stations 1 and 3).

B) Field data were collected primarily to the west of Seal Bend.

C) Three transects measuring eelgrass density were collected by divers and include the 18 validation points used in the study.

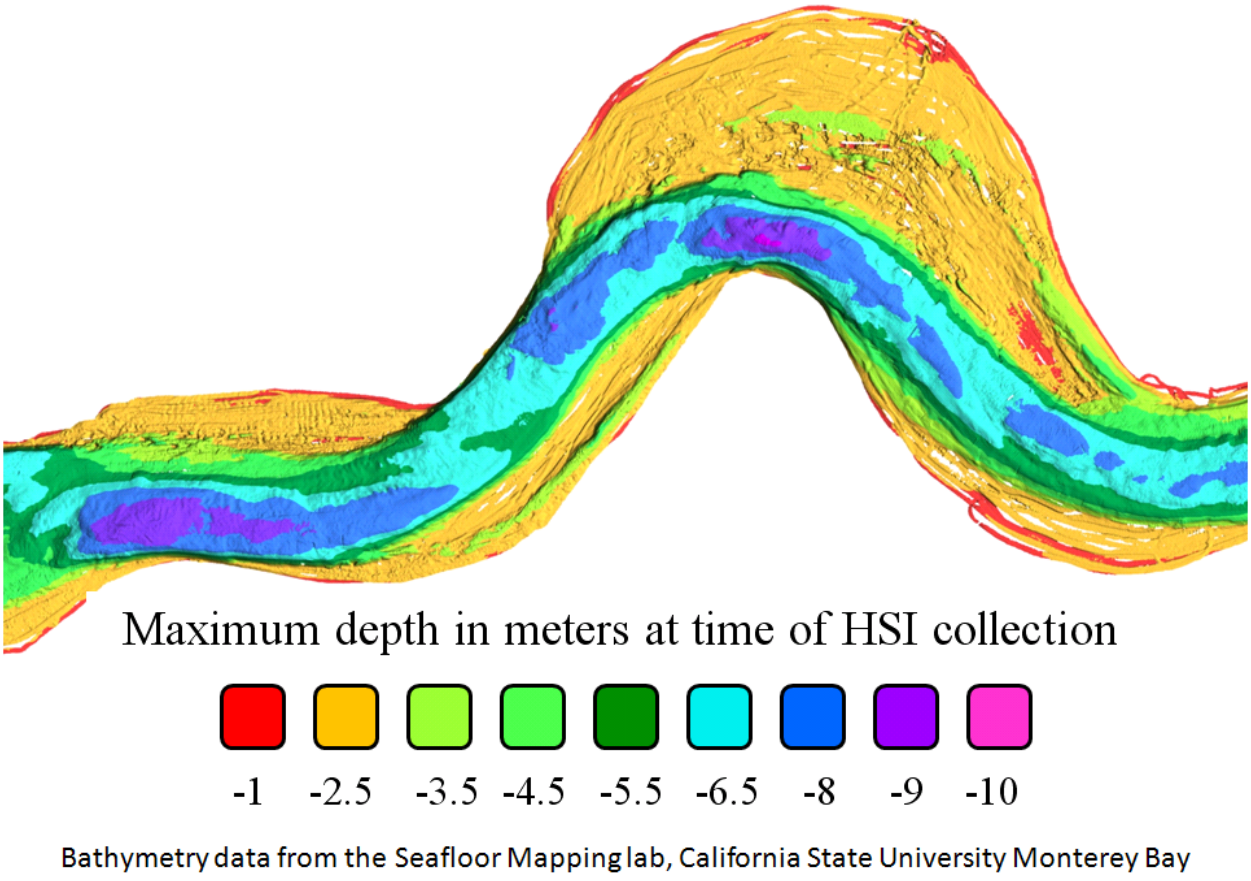

Figure 4 Bathymetry of Elkhorn Slough

Bathymetry of Elkhorn Slough at the time of image collection corresponding to high slack tide. Suitable habitat for eelgrass includes depths from -1 to -3.5 m, including the red, orange, and light green areas of the map. A deep channel (deeper than -5.5 m) runs through the center of Elkhorn Slough with higher current flow and no eelgrass.

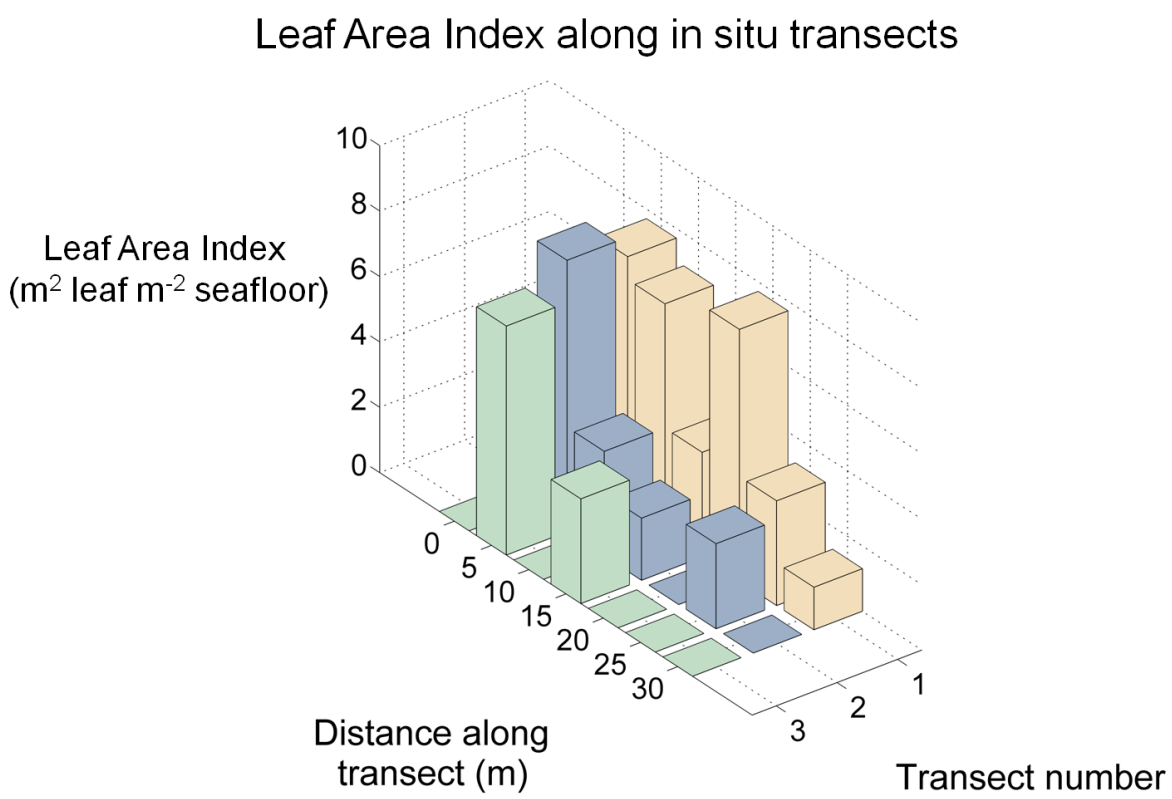

Figure 5 Leaf Area Index along transects

The distribution of eelgrass Leaf Area Index (LAI) measured along the three transects shows a patchy distribution with considerable variability between dense eelgrass (LAI=6-8), sparse eelgrass (LAI=1-4), and sediment (LAI=0).

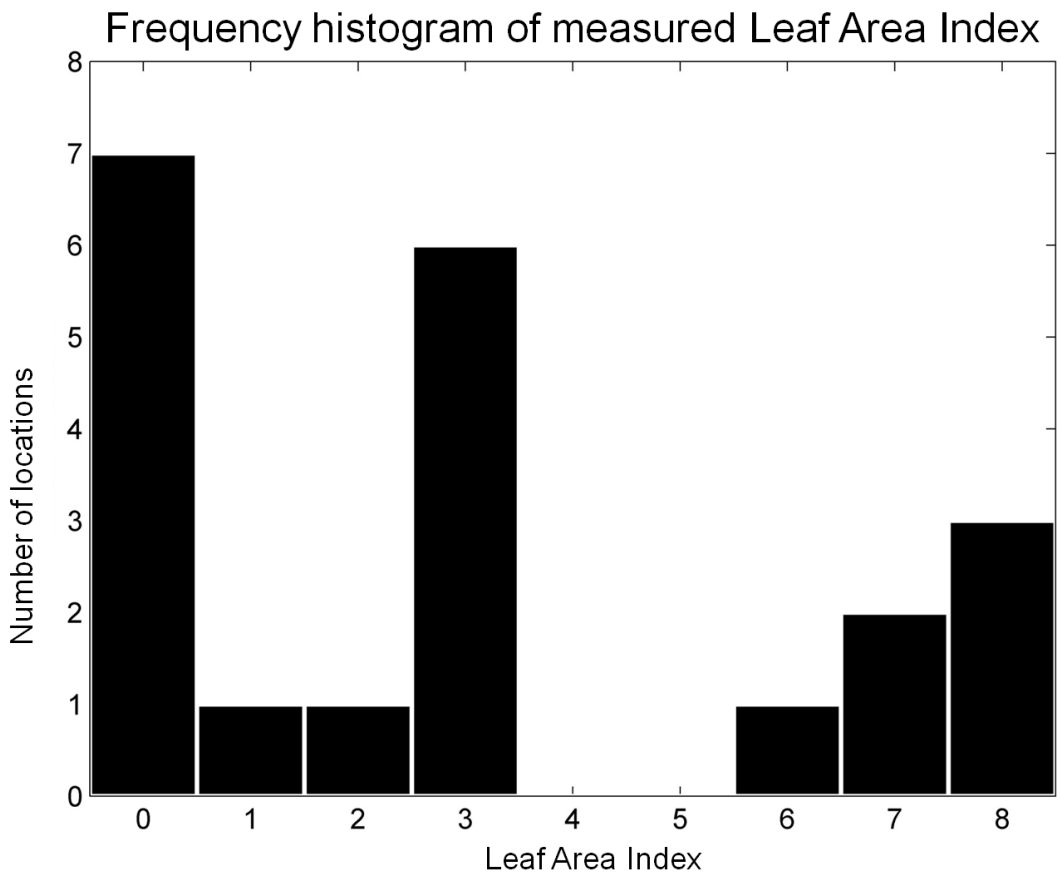

Figure 6 Frequency histogram of Leaf Area Index

The number of field stations containing eelgrass with Leaf Area Indices ranging from dense (6-8) to sparse (1-4) to sediment (0).

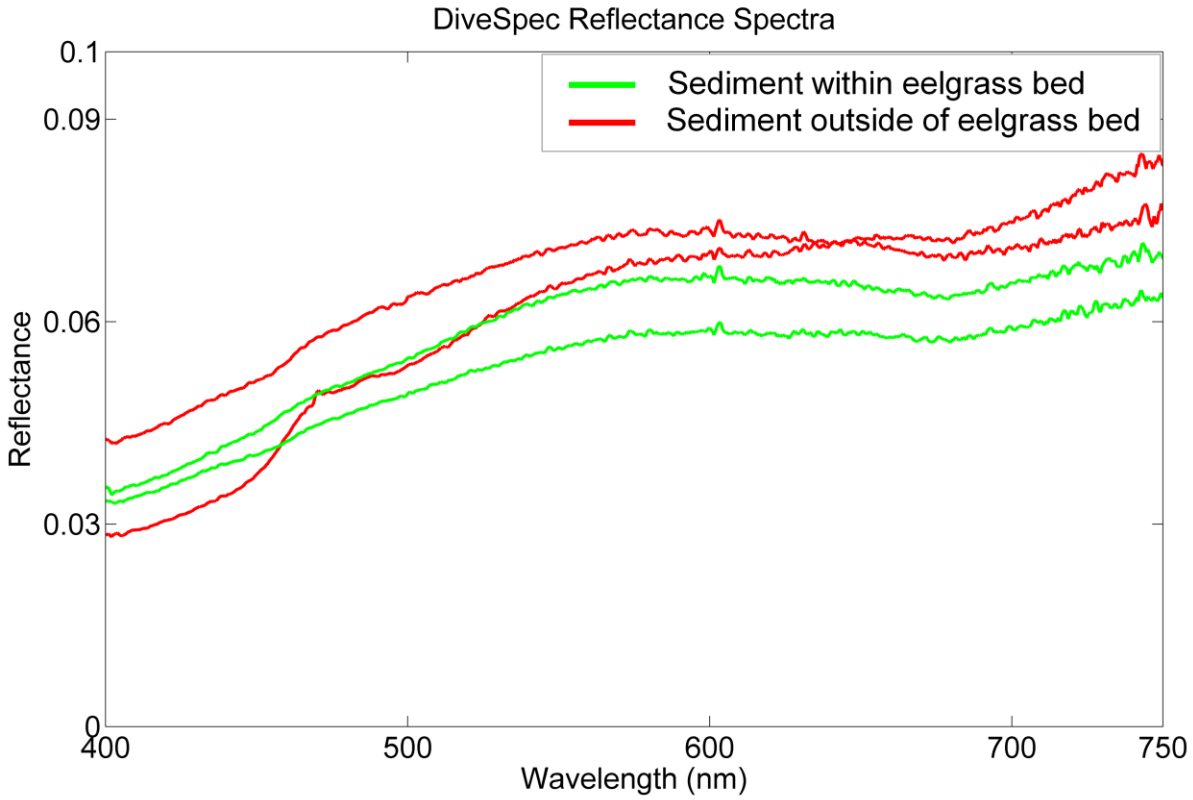

Figure 7 DiveSpec reflectance spectra

Reflectance of sediment measured by divers both within and outside the eelgrass beds.

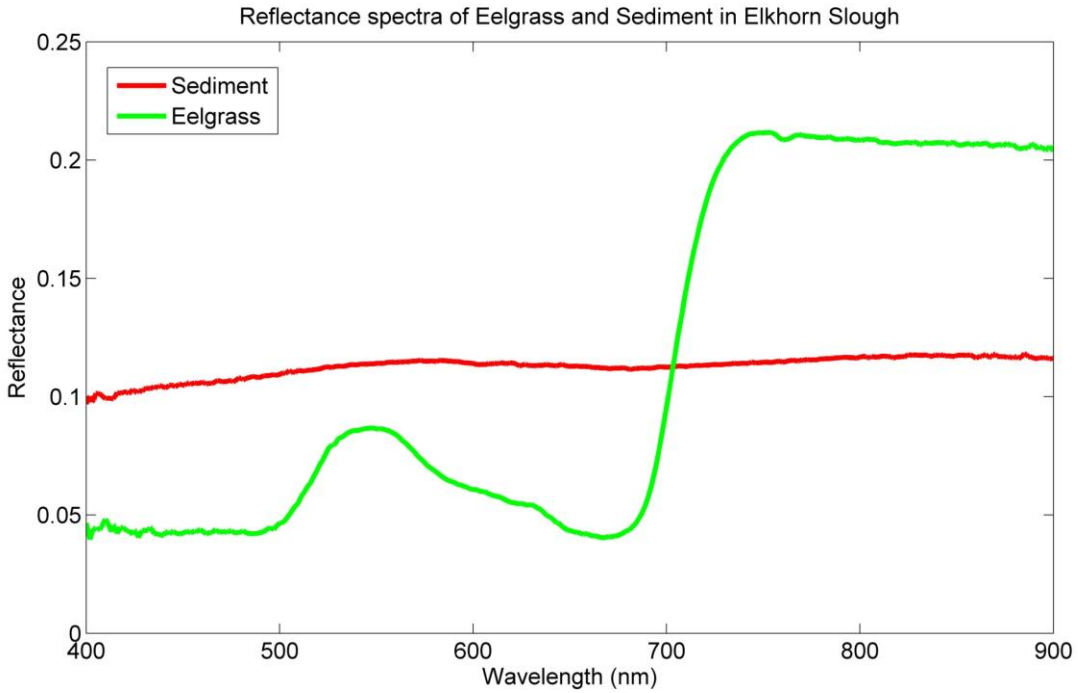

Figure 8 Reflectance of eelgrass leaf and sediment core

Reflectance spectra were measured in the laboratory from a sediment core and an eelgrass leaf.

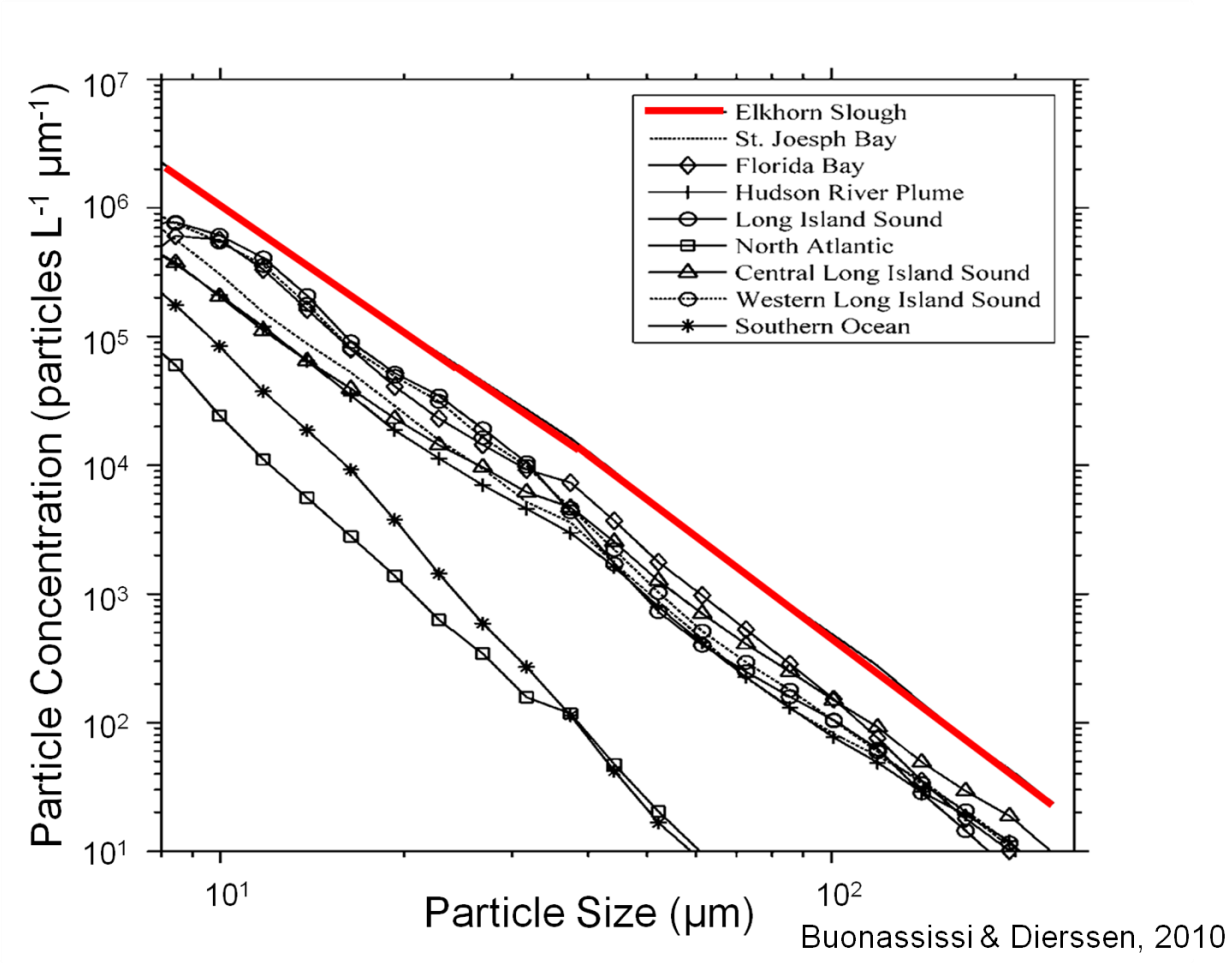

Figure 9 Particle size distributions in Elkhorn Slough compared to other bodies of water

Measurements of particle size distributions (particle diameter versus concentration) from water collected throughout the world. The particle concentrations from Elkhorn Slough are higher than other estuaries, including Long Island Sound, indicating a very turbid particle-laden water body.

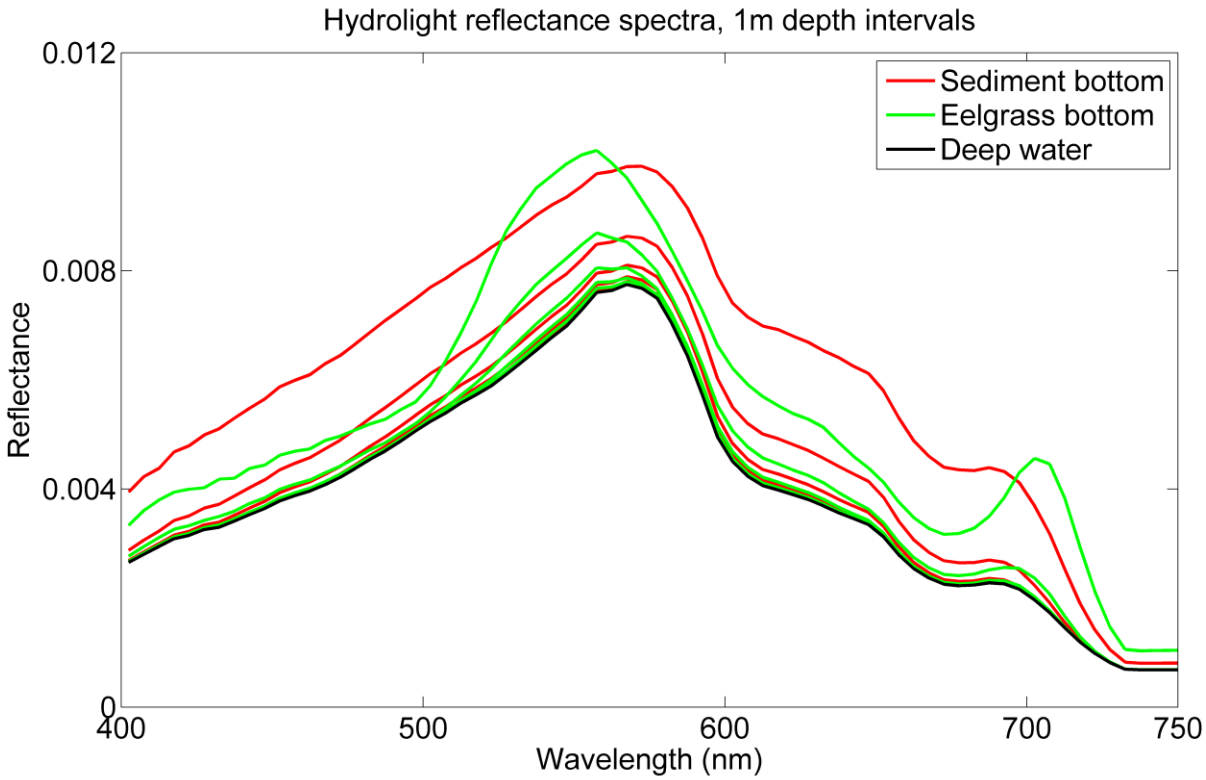

Figure 10 Remote sensing reflectance modeled for different bottom types

Remote sensing reflectance (sr^{-1}) modeled with measured water column properties and different types of seafloor constituents. Three lines are shown for sediment and eelgrass corresponding to different water depths of 1 m (top line), 2 m (middle line), and 3 m (bottom line). The modeled spectrum for deep water, shown in black, is indistinguishable from eelgrass or sediment at 4 m depth.

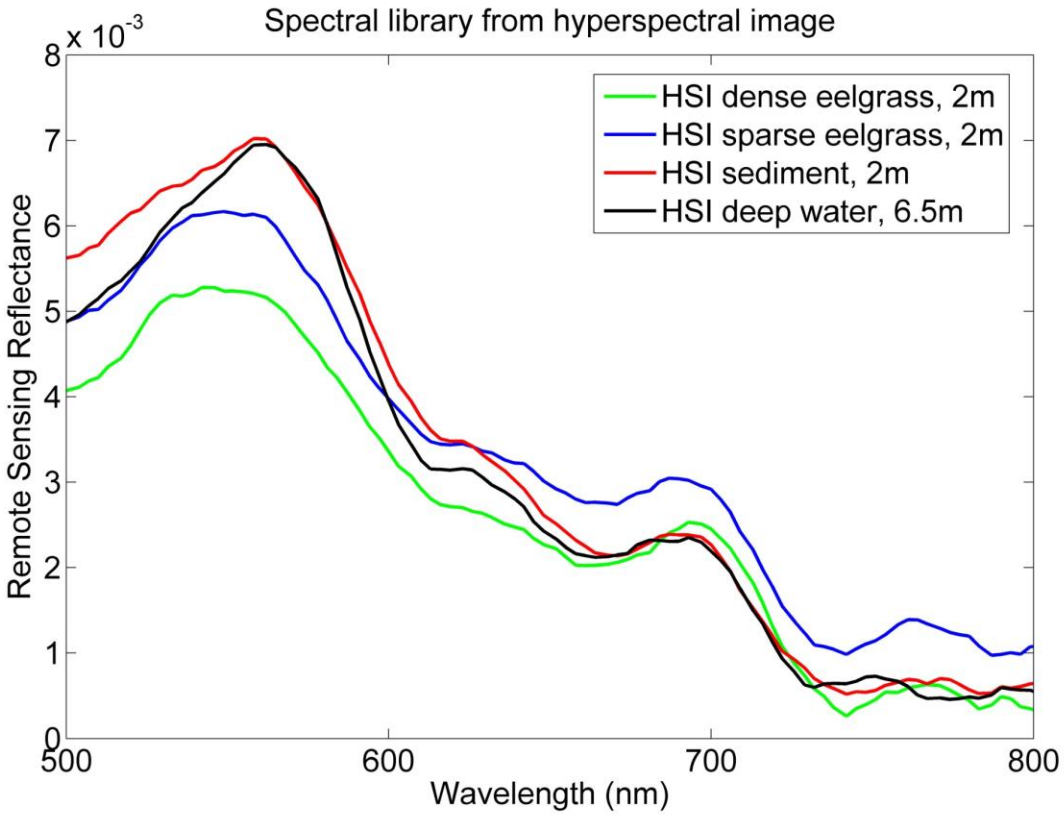

Figure 11 Spectral library of image-based endmembers

Remote sensing reflectance (sr^{-1}) from the hyperspectral imagery was used to create a spectral library. The selected endmembers include dense eelgrass (LAI = 7.0), sparse eelgrass (LAI = 3.2), and bare sediment all at approximately 2 m depth. A spectrum describing deep water was taken from the deep channel at a depth of 6.5 m.

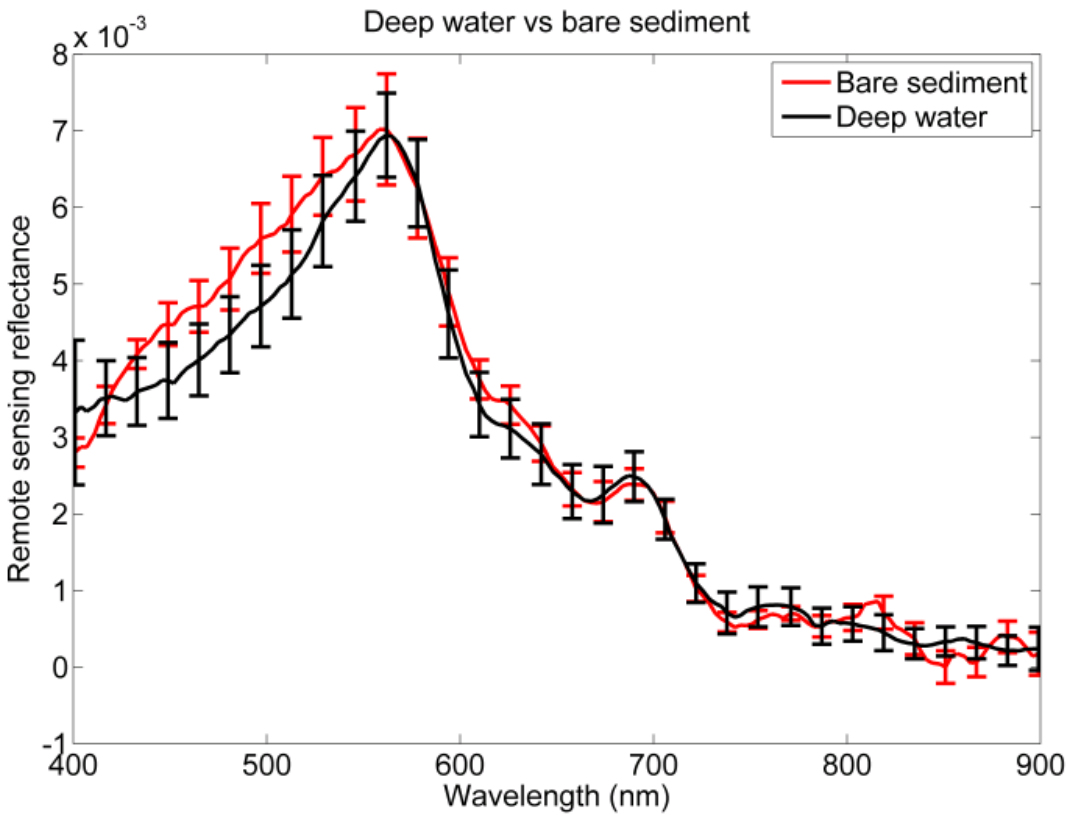

Figure 12 Standard errors in sediment and deep water spectra

The average remote sensing reflectance (sr^{-1}) spectrum with one standard error for all field stations containing bare sediment on the seafloor (<3 m water depth) compared to a similar number of deep water (>5.5 m water depth) pixels. The overlap of error bars across the visible spectrum indicate no significant difference between two spectra and show that deep water and sediment cannot be spectrally distinguished.

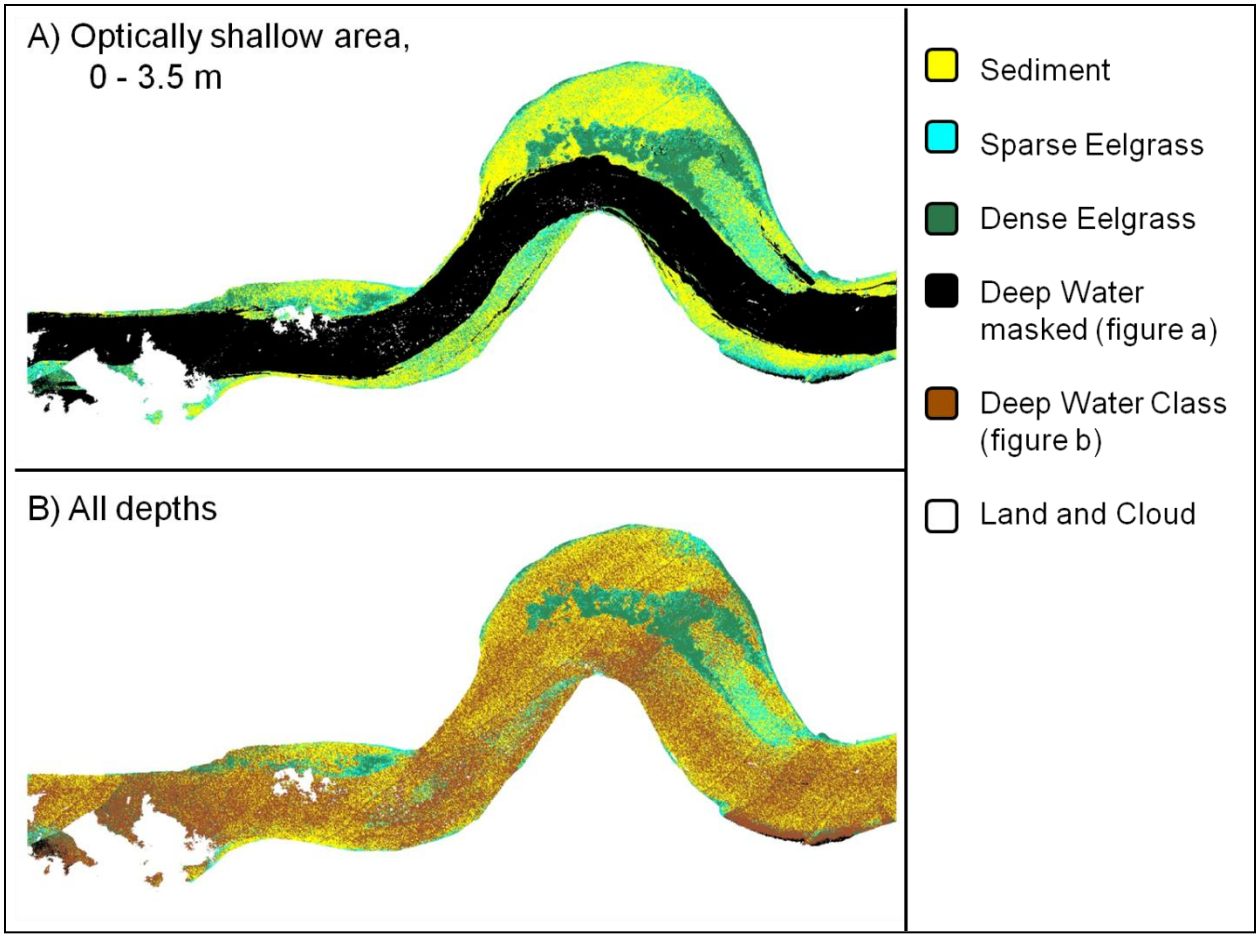

Figure 13 Eelgrass classification from the hyperspectral imagery

A) Eelgrass was mapped from the hyperspectral imagery using the spectral information divergence classification algorithm and a spectral library with image-based endmembers with the deep channel masked in black.

B) Without masking the deep water, the classification approach can map the eelgrass beds but cannot distinguish bare sediment (yellow) from deep water (brown).

		Image Classification						
Ground Truth Data		dense eelgrass	sparse eelgrass	bare sediment	total possible	omissions	commissions	mapping accuracy
	dense eelgrass	5	0	0	5	0	5/10	100%
	sparse eelgrass	3	2	2	7	5/7	0	29%
	bare sediment	2	0	4	6	2/6	2/6	67%
	total	10	2	6	18			61%

Figure 14 Classification accuracy matrix

Accuracy matrix of the classification shown in **Error! Reference source not found.**A for the 18 alidation data points ranging from dense eelgrass to bare sediment. The boxes in red indicate agreement between the image classification and the validation data points of 61% (11/18). All five of the locations with dense eelgrass were correctly located, and four of the six locations with sediment. Sparse eelgrass was only classified with 29% accuracy.

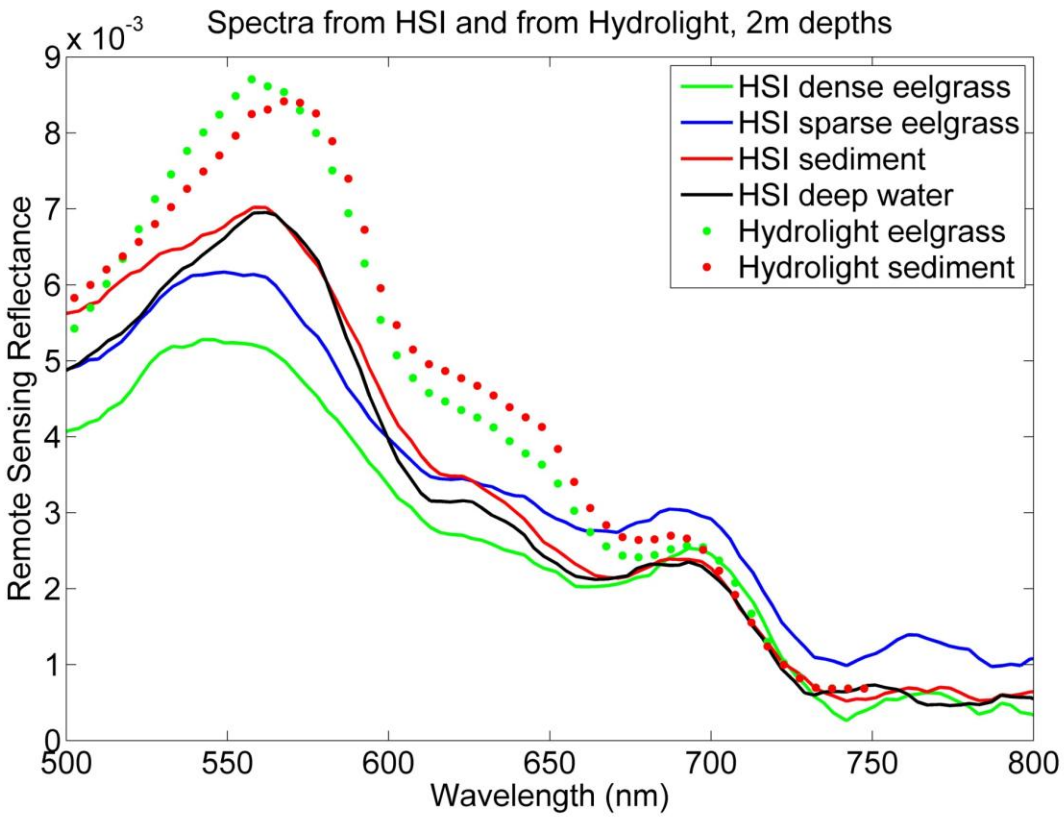

Figure 15 Comparison of spectra from the hyperspectral imagery and radiative transfer model

Remote sensing reflectance (sr^{-1}) for stations containing eelgrass and sediment bottoms from the radiative transfer model (dotted lines) were higher in magnitude than the spectra from the hyperspectral image (solid lines).

Figure 16 Glint visible in the hyperspectral imagery

A pseudo true color image of the study location from the SAMSON imagery shows differences in the magnitude of reflected light due to sun glint between the NE/SW flight track lines (arrows).

Figure 17 Historical imagery from Google Earth

An aerial photograph or image of Elkhorn Slough, CA taken 25 May 2006 by Digital Globe available in the Google Earth archive.

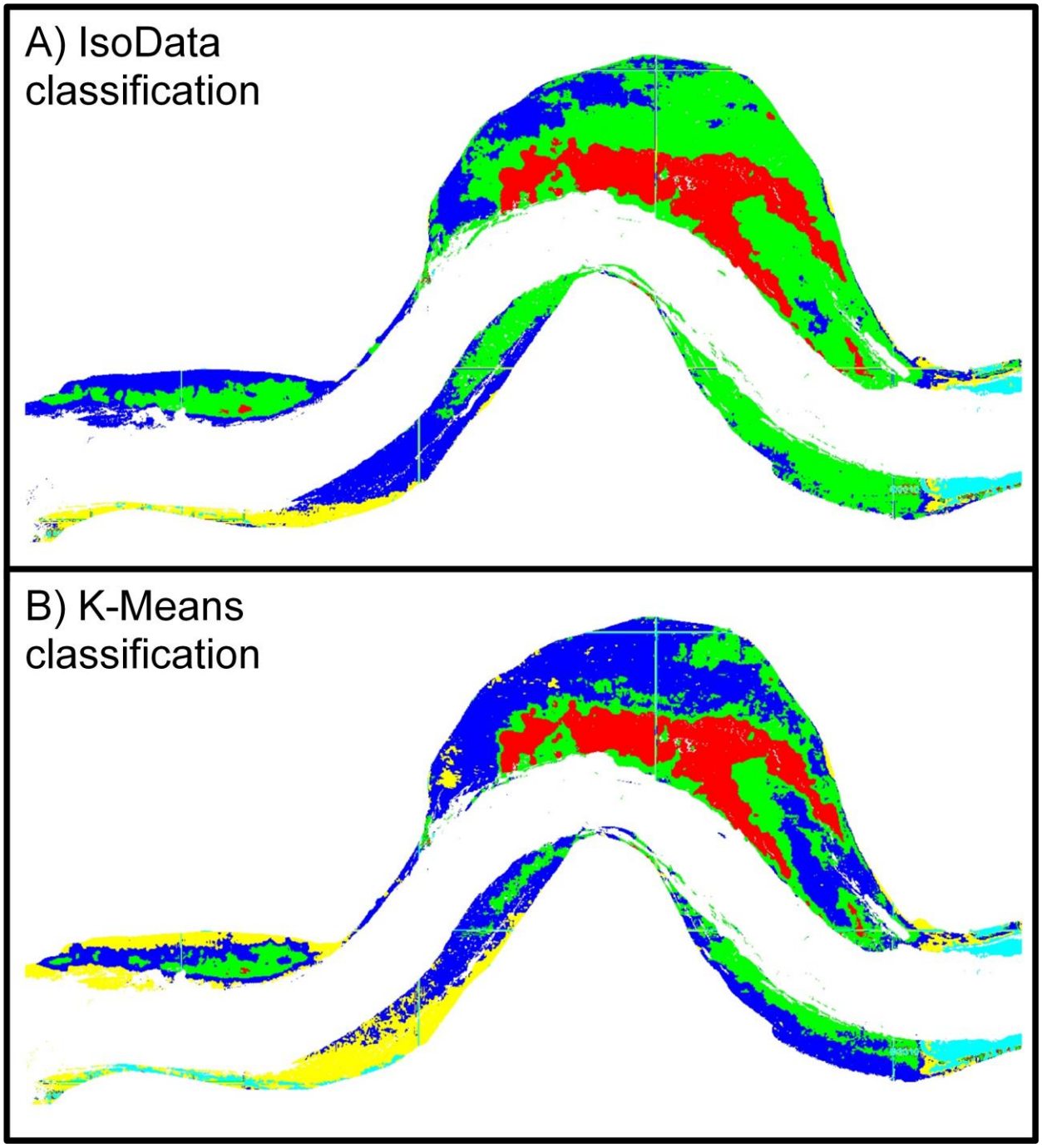

Figure 18 Results of unsupervised classification of Google Earth imagery

Both unsupervised classification algorithms show the general shape of the main eelgrass bed in the central Seal Bend, but classify eelgrass in the smaller bed to the west in the same class as sediment in the central bed (green).

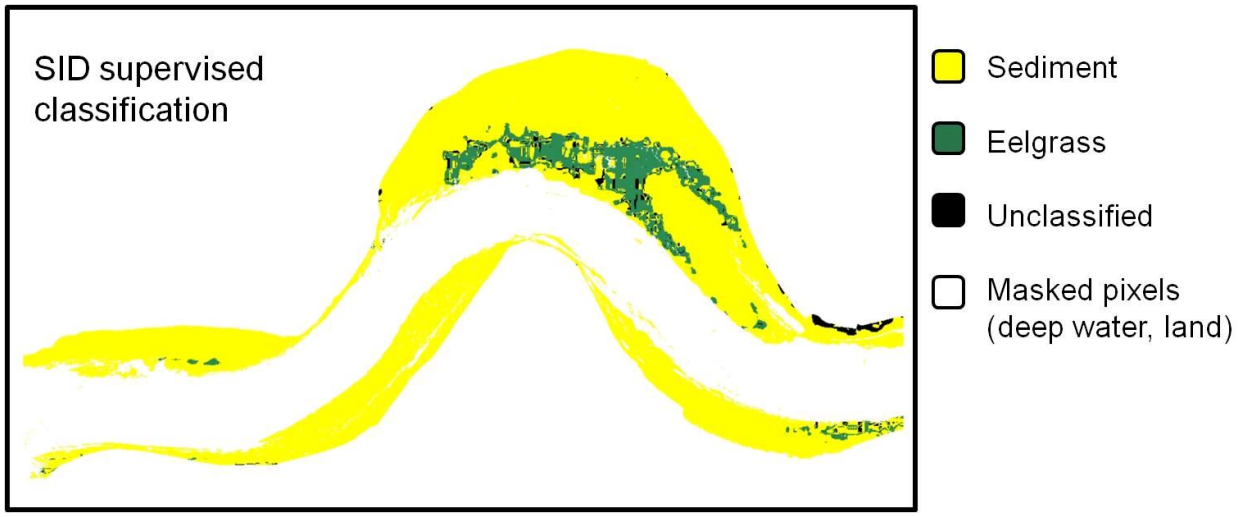

Figure 19 Results of supervised classification of Google Earth imagery

The presence and absence of eelgrass appears appropriately classified in the eelgrass bed in Seal Bend, but the smaller bed in the western part of the Slough is significantly smaller than expected.